applied sciences

MDPI

Article

Study on Surrounding Rock Control of Withdrawal Space in Fully Mechanized Caving Mining of a 19 m Extra-Thick Coal Seam

Dongdong Chen [1], Zhiqiang Wang [1], Shuaishuai Yue [2,*], Shengrong Xie [1], Fulian He [1], Chunyang Tian [1], Zaisheng Jiang [1], Dawei Liang [1] and Bohao Qi [1]

[1] School of Energy and Mining Engineering, China University of Mining and Technology-Beijing, Beijing 100083, China
[2] School of Energy Science and Engineering, Henan Polytechnic University, Jiaozuo 454003, China
* Correspondence: yueshuaishuai@hpu.edu.cn

Abstract: The section span of the withdrawal space of fully mechanized top coal caving in an extra-thick coal seam is large, and with the gradual withdrawal of the hydraulic support, a series of strong dynamic pressure disasters occur in the withdrawal space, and the difficulty of surrounding rock support control increases sharply. In order to study the control mechanism of surrounding rock in the final mining withdrawal space in detail and put forward a reasonable support technology scheme, taking the large-section withdrawal space of an 8309 fully mechanized caving face in an extra-thick coal seam of a mine as the research object—through the theoretical investigation of whether the key blocks of the main roof are stably hinged under varied stopping coal caving distances and fracture locations of the main roof—the reasonable and optimal stopping coal caving distances and roadway formation time are determined. Using numerical simulation and similar simulation methods, the vertical stress and the maximum shear stress research indicators were introduced to verify the accuracy of the theoretical analysis results. The results show the following: (1) The reasonable stopping coal caving span is 1~2 times the cycle weighting interval, the best stopping coal caving distance in this geological condition is 30 m, and the best fracture position of the main roof is located above the goaf. (2) The migration of overlying strata in the withdrawal space has obvious zoning characteristics, and the zoning is as follows: a stopping coal caving area, support area of the hydraulic support, withdrawal channel area, and stopping coal pillar area. (3) According to the zoning characteristics of overlying strata movement, the asymmetric zoning support control scheme of the withdrawal space is proposed. The field monitoring results show that the maximum roof subsidence in the withdrawal space is 151 mm, the maximum internal squeezing amount of the stopping coal pillar is 82 mm, and the supporting and anchoring effect of each partition in the withdrawal space is good. The set of partition asymmetric support control schemes has been successfully applied to field practice.

Keywords: top coal caving; extra-thick coal seam; withdrawal space; final mining; coal caving distance; fracture position; asymmetric zoning

check for updates

Citation: Chen, D.; Wang, Z.; Yue, S.; Xie, S.; He, F.; Tian, C.; Jiang, Z.; Liang, D.; Qi, B. Study on Surrounding Rock Control of Withdrawal Space in Fully Mechanized Caving Mining of a 19 m Extra-Thick Coal Seam. *Appl. Sci.* **2024**, *14*, 9694. https://doi.org/10.3390/app14219694

Academic Editor: Tiago Miranda

Received: 27 August 2024
Revised: 3 October 2024
Accepted: 17 October 2024
Published: 23 October 2024

Copyright: © 2024 by the authors. Licensee MDPI, Basel, Switzerland. This article is an open access article distributed under the terms and conditions of the Creative Commons Attribution (CC BY) license (https://creativecommons.org/licenses/by/4.0/).

1. Introduction

China is rich in coal resources, among which the reserves of thick and extra-thick coal seams account for more than 40% of China's coal reserves [1,2]. Thick and extra-thick coal seams are the main mining coal seams in China at this stage. With the continuous improvement of fully mechanized caving surrounding rock control systems [3–6] and the continuous improvement of underground mechanization and intelligence [7–10], fully mechanized top coal caving mining is widely used in underground thick coal seam mining because of its low cost and high yield, effectively reducing the number of working face moves and other advantages. However, there are many problems in the final mining stage

of extra thick coal seam, such as the coal recovery rate being low [11,12], the working face being under severe pressure, and the support withdrawal being blocked [13,14].

Many scholars and experts have conducted research on the overburden structure [15–17], the law of mine pressure behavior [18–20], and the final mining withdrawal process [21] of the extra-thick fully mechanized caving face. In order to solve the problem of serious floor heave in water-bearing soft rock roadway, Sakhno et al. [22] used an indoor test, numerical simulation, and other research methods to study the mechanism of floor heave and the difference in grouting schemes with five different reinforcement depths, and finally obtained the reliable conclusion that the grouting depth is determined by floor heave and water content. Aiming at the problems of complex overburden rock migration and the difficult control of surrounding rock in steeply inclined and extra-thick coal seam mining, Wang et al. [23] used a variety of research methods to analyze the characteristics of overburden rock migration under geological conditions, and the research results achieved safe and efficient mining of fully mechanized caving. Cui et al. [24] used a variety of research methods to demonstrate that surface filling is a reliable means to control the influence of strong mining in the thick coal seam under a complex overburden environment. In the technology of gob-side entry retaining in fully mechanized caving mining, Kong et al. [25] established a mine pressure model, numerical model, and similar model of keeping an alley along empty space under the condition of top coal caving mining, and summarized the stress evolution characteristics between the top coal and filling body and the influence of different top coal conditions on the stability of keeping an alley along empty space. Li et al. [26] studied the injury degrees of surrounding rock in a shallow fully mechanized caving mining face by using borehole peeping and CT scanning technology. Tu et al. [27] established a mechanical model in the fully mechanized top-coal caving mining of an extra-thick island working face and deduced the mechanical equation of mining stress distribution and failure depth of coal rock under this geological condition. Zhao et al. [28] determined the distribution range of an internal and external stress field and the reasonable layout position of roadway by studying the overburden structure and stress evolution characteristics of extra-thick fully mechanized caving mining. Based on the problem of asymmetric deformation and failure of gob-side entry in a fully mechanized caving face, Xu et al. [29] used a variety of research methods to analyze the stress evolution and plastic deformation mode of coal pillar roadway, and put forward the asymmetric high pre-tightening force support scheme.

From different research perspectives, the above scholars have performed effective research on the overburden structure, mine pressure behavior laws, and support control of mining roadway in extra-thick fully mechanized caving face using different research methods. The final mining working face involves the problem of safe withdrawal. In order to ensure the orderly replacement of the working face, it is necessary to pre-excavate or use the self-excavation withdrawal channel of the shearer to facilitate the withdrawal of the support. The withdrawal channel is connected with the support area of the hydraulic support to form a large-section withdrawal space. The withdrawal space has a control problem, with large span and difficult support. However, there is a lack of targeted research on the stress evolution law of the withdrawal space at the final stage of the fully mechanized top coal caving mining, the structural characteristics of the overlying strata, and the support control problem. Therefore, this paper takes the withdrawal space of the 8309 fully mechanized top coal caving face of a mine as the research background. Through numerical simulation and physical similarity simulation experiments, the following aspects are studied: how to optimize the stop caving distance to improve the coal recovery rate; how to use the migration law of the large structure of the overlying strata to reduce the pressure appearance degree of the withdrawal space at the final stage of mining; and how to improve the support control of the withdrawal space to ensure the safe withdrawal of the support.

2. Engineering Background

2.1. The 8309 Working Face Overview

The main mining of the 8309 extra-thick fully mechanized caving face is the 3~5# coal seam. The average buried depth of the test object is 575 m, the average dip angle is 0~3°, the average coal thickness is 19.0 m and the coal thickness is evenly distributed. The 8307 working face in the adjacent section has been mined out stably and 40 m coal pillars are left between the sections. Therefore, the mining of the adjacent working face has a very weak influence on the normal mining of the test working face and the disturbance of the final mining withdrawal support. The four-neighbor relationship of the 8309 working face is shown in Figure 1.

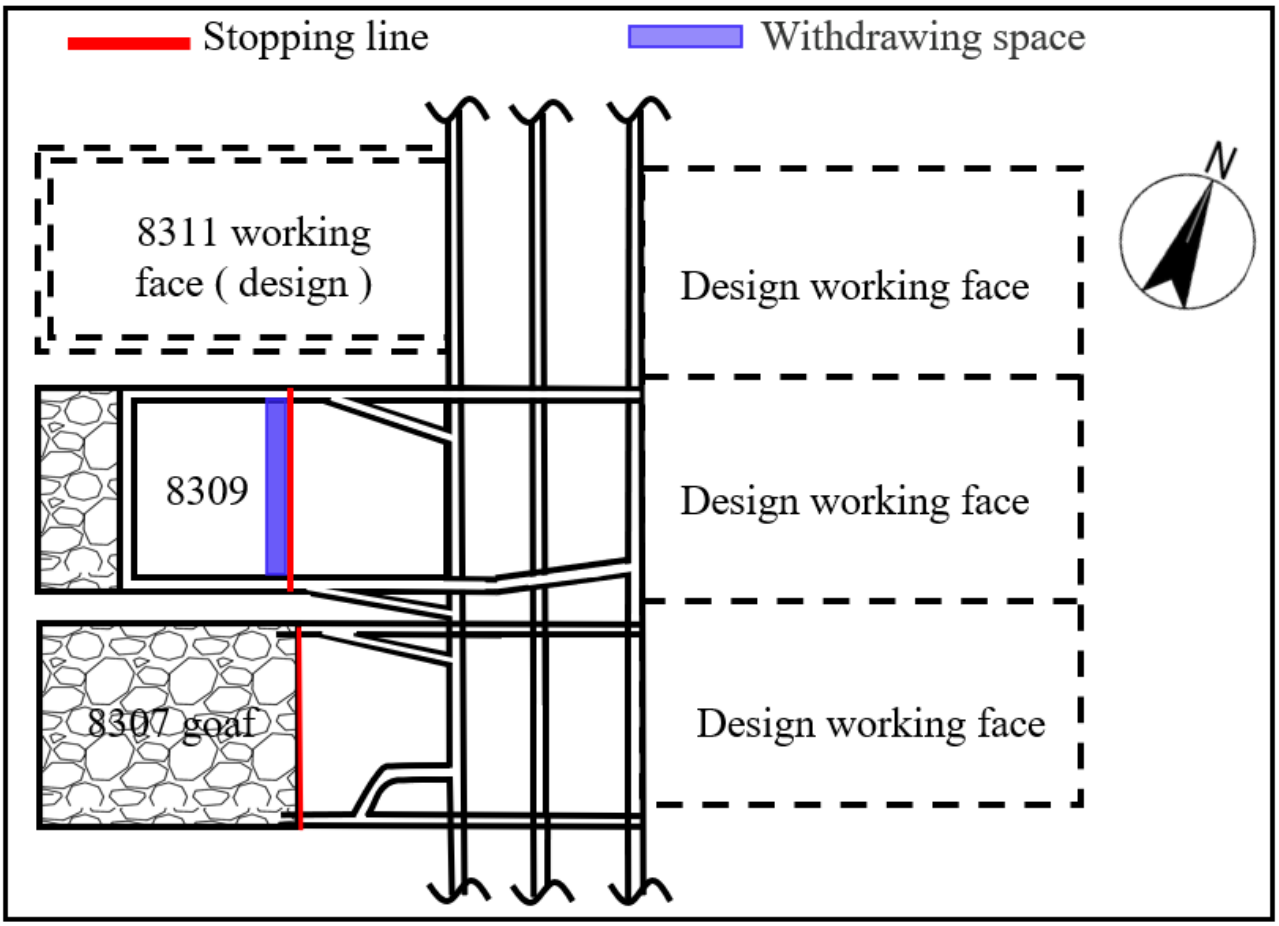


Figure 1. The four-neighbor relationship of the 8309 working face.

The mechanized mining height of the 8309 working face is 3.5 m, the height of top coal is about 15.5 m, and a withdrawal channel with a width of 3.8 m and a height of 3.5 m is constructed behind the stop line. In this paper, the support area of the hydraulic support and the withdrawal channel area are collectively referred to as the (large section) withdrawal space. A comprehensive histogram of coal and rock strata in the 8309 working face is shown in Figure 2.

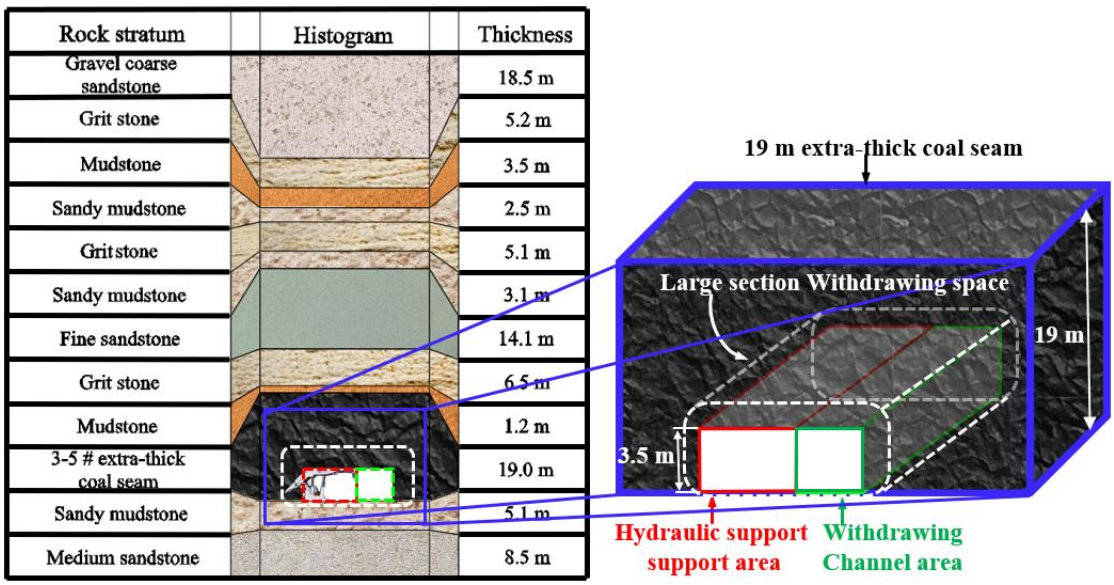


Figure 2. Comprehensive histogram of coal and rock strata.

2.2. Evaluation of the Original Stopping Technology and Support Control Effect

It is known that the cycle weighting interval distance of the final mining of the typical fully mechanized caving face is about 26 m under similar geological conditions. Through field investigation of the typical extra-thick fully mechanized caving face, it is found that in the original final mining stopping coal caving distance, the design and construction of the withdrawal space support control have the following problems: In the actual mining process, the stopping coal caving distance is not less than 50 m, and the long-distance stop caving operation seriously wastes coal resources. The support strength is the same everywhere in the withdrawal space, and the original support control is not targeted. The key points of support control in each area of the withdrawal space are not clear, and the difference in overburden rock migration structure and support control in each area during the final mining and parking period is not considered. At the same time, the reasonable operation time of stopping coal caving has not been grasped, and it is not recognized that the fracture position of the main roof is very important for the effective support control of the withdrawal space and the safe withdrawal of the working face support. Therefore, both stopping coal caving operations in the final mining stage and rationally optimizing the stopping coal caving scheme are beneficial to the economic and efficient mining of the working face.

3. Theoretical Analysis of Surrounding Rock Stability in the Withdrawal Space at the Final Mining of Fully Mechanized Caving

3.1. The Mechanism of Stopping Coal Caving in Fully Mechanized Caving Final Mining

Stopping coal caving operations provides a stable overburden environment for the safe withdrawal of the final mining face and the withdrawal space. In line with the description, this paper divides the typical key rock blocks of the main roof into A, B, C_1, C_2, and C_3. Coal caving is not stopped in the final mining stage (Figure 3a). Due to the large space in one-time mining, the direct roof above the goaf cannot enrich the goaf, the main roof suspension begins to break to a certain extent, and B rotates and sinks. Due to the increase in the rotation angle of B and the decrease in the overlap width between B and the stopping coal pillar, when the coal wall and the overlying direct roof yield and plasticize to a certain extent until they cannot withstand the disturbance of the rotation and extrusion of B, the coal wall and the overlying direct roof collapse, and A and B cannot maintain a stable hinged state for a long time. At the same time, the collapse gangue is squeezed into the working face, and the shield beam of the hydraulic support is greatly increased by load,

which makes it difficult to withdraw the support. If the coal caving is stopped in the final mining stage (Figure 3b), only 3.5 m is mined, and the remaining uncaving coal and direct roof caving are filled in the goaf. B only rotates at a small angle and sinks into the gangue, under the joint support of the stopping coal pillar and the caving gangue in the goaf, and A, B, and C_1 form a stable hinged structure. Most of the dynamic and static load stress generated by B rotation acts on the stopping coal caving filling area behind the support, which greatly weakens the damage effect of B rotation on the stable bearing structure of the overlying strata in the withdrawal space. The indication of whether to stop coal caving in the final mining stage is shown in Figure 3.

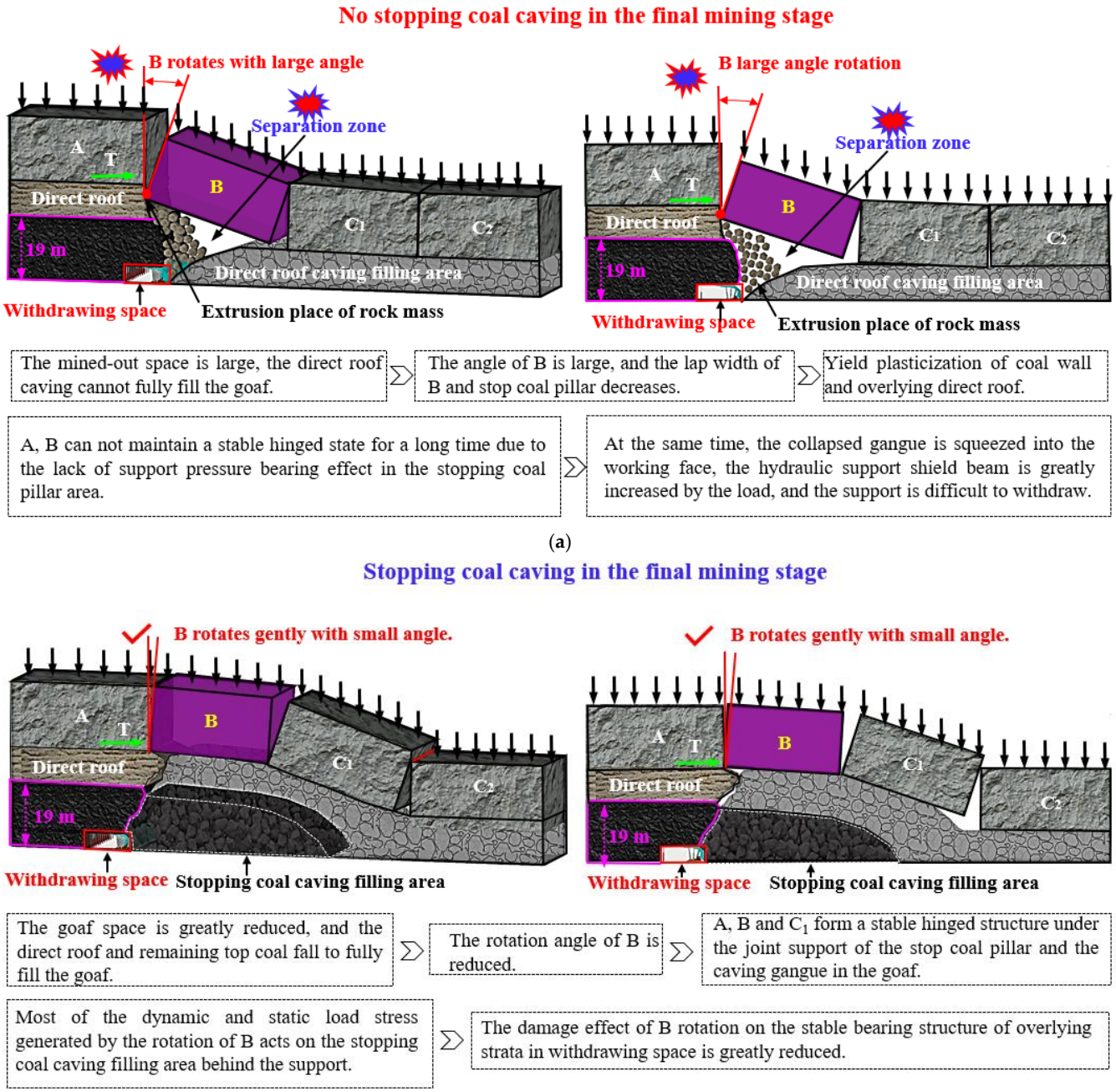


Figure 3. A schematic diagram of whether to stop coal caving in the final mining stage: (**a**) No stopping coal caving in the final mining stage; (**b**) stopping coal caving in the final mining stage.

3.2. Stability Analysis of Key Blocks of Overlying Strata in the Withdrawal Space

The stability of the hinged structure between the key blocks is related to the stability of the overlying strata in the withdrawal space and the safe withdrawal of the support. In order to clarify the difference in the stability of the hinged structure of the key blocks with or without stopping coal caving and at different stopping coal caving distances, the theoretical calculation and analysis of the stability of the key blocks of the overlying strata in the final withdrawal space are carried out.

3.2.1. Theoretical Analysis of Reasonable Stopping Coal Caving Distance

Reasonable stopping coal caving distance can slow down the rotation angle of fractured rock mass, weaken the influence of the dynamic and static load's combined disturbance on the stable overburden environment of underlying withdrawal space during the rotation and subsidence of key blocks, and ensure the safe and efficient withdrawal of final mining hydraulic support. The selection principle of reasonable stopping coal caving distance is as follows: on the one hand, ensure that the goaf area below B is fully filled, and the rotation angle of B is small; on the other hand, the uncaving top coal and the caving direct roof collapse and slip to the lower part of C_1 under the action of the B rotary extrusion and fill part of the goaf space below C_1. The rotation angle of C_1 is larger than that of B to a certain extent but it can ensure the transition to B and C_2 and ensure the stable hinge between the key blocks. Therefore, the selection of stopping coal caving distance is closely related to the strike length (L_Z) of the fractured rock mass of the final mining. In this paper, the L_Z approximate the cycle weighting interval distance of the final mining period (26 m). The distance of stopping coal caving is summarized into the following four types—a: $L_C = 0$ m; b: $0 < L_C < L_Z$; c: $L_Z \leq L_C < 2L_Z$; d: $L_C \geq 2L_Z$. Under the four typical stopping coal caving distances, the migration of the key blocks of the overlying basic roof in the withdrawal space is shown in Figure 4.

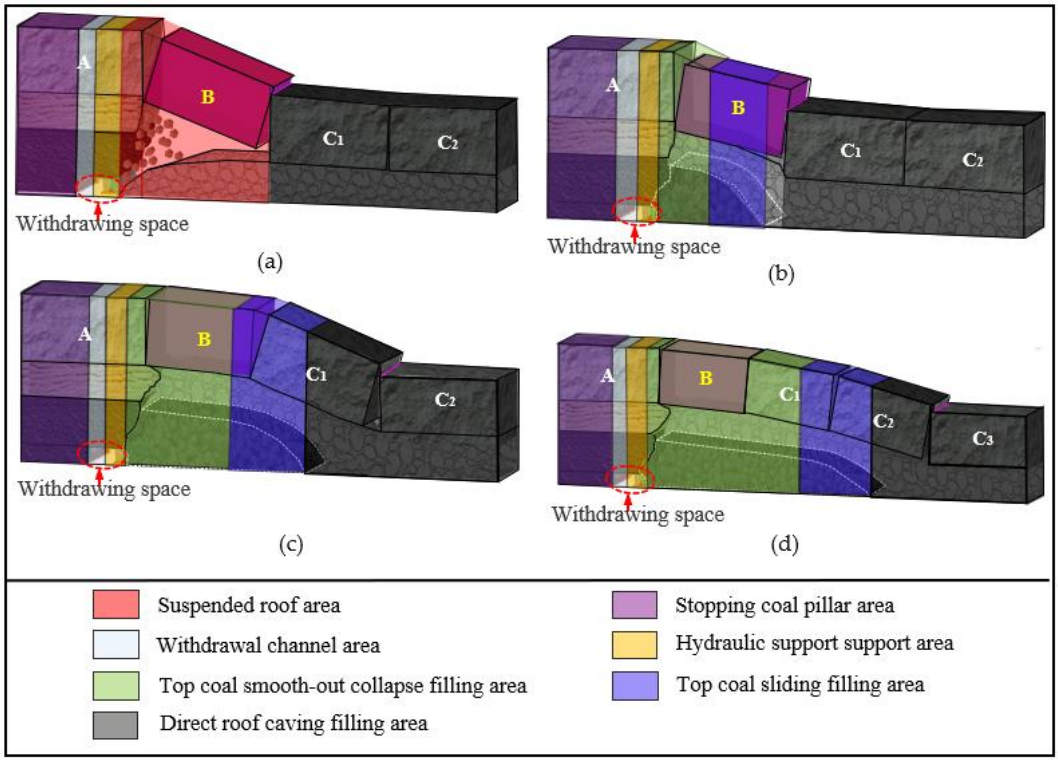


Figure 4. Overburden rock migration characteristics of withdrawal space in different stopping coal caving spans: (**a**) $L_C = 0$ m; (**b**) $0 < L_C < L_Z$; (**c**) $L_Z \leq L_C < 2L_Z$; (**d**) $L_C \geq 2L_Z$.

(1) When L_C = 0 m (Figure 4a), B has a large rotation angle. After the hinges of B and C_1 are stable, there is still a large area of goaf space below B. In order to facilitate the subsequent corresponding regional analysis, according to the migration of the main roof fracture rock mass in the withdrawal space, the overlying rock in the withdrawal space can be divided into a stopping coal pillar area, a support area of the hydraulic support, withdrawal channel area, suspended roof area, and direct roof caving filling area.

(2) When $0 < L_C < L_Z$ (Figure 4b), the rotation angle of B gradually decreases with the increase in stopping coal caving distance. However, due to the limited stopping coal caving distance, the range of top coal slow collapse and sliding filling goaf is limited, and the vertical dislocation difference between B and C_1 is large. There are still some suspended roof areas in the goaf below B and C_1. With the continuous advancement of the final mining face, the hinged structure cannot maintain a stable state for a long time, which is not conducive to the stable migration of the final mining overburden. According to the migration of the main roof fracture rock mass in the withdrawal space, the overlying strata in the withdrawal space are divided into a stopping coal pillar area, support area of the hydraulic support, withdrawal channel area, top coal smooth-out collapse filling area, top coal sliding filling area, suspended roof area, and a direct roof caving filling area.

(3) When $L_Z \leq L_C < 2L_Z$ (Figure 4c), the rotation angle of B is obviously slowed down under the buffer support of the caving coal and rock mass. Due to the effect of the rotary extrusion pressure of B, the caving top coal slips and fills the goaf below C_1, and the rotation angle of C_1 slows down. The B rotation subsidence is supported by C_1, and the C_1 rotation is buffer supported by the rear C_2. According to the migration of the main roof fracture rock mass in the withdrawal space, the overlying strata in the withdrawal space are divided into the stopping coal pillar area, the support area of the hydraulic support, withdrawal channel area, top coal smooth-out collapse filling area, top coal sliding filling area, and direct roof caving filling area.

(4) When $L_C \geq 2L_Z$ (Figure 4d), the rotation angle of B and C_1 under the buffer support of the caving coal and rock mass is obviously slowed down. Due to the long distance to stop coal caving, the caving top coal slides and fills part of the goaf below C_2 but C_2 can be stable under the action of direct roof caving and filling, therefore, the long-distance parking of top coal is a serious waste of coal resources.

In summary, when the stopping coal caving distance satisfies $L_Z \leq L_C < 2L_Z$ (Figure 4c), it can not only ensure that B is stably hinged with A and C_1 but it also reduces the coal loss rate to a certain extent. It is proposed that the distance of stopping coal caving is 26 m, and the maximum distance of uncaving top coal under extrusion and caving meets Formula (1) [30]:

$$L = LC + \frac{h_2}{\sin\theta} - h_j \cot\alpha \quad (1)$$

In this context, L is the distance from the farthest point of uncaving top coal to the hydraulic support; L_C is the distance to stop coal caving, 26 m; θ is the top coal caving fracture angle, 60°; α is the inclination angle of the shield beam of the support, 60°; h_2 is the height of uncaving top coal, 15.5 m; h_j is the mining height of coal seam, 3.5 m.

The L is 41.8 m. Considering that the coal quality of the coal body is relatively hard, some coal and rock masses near the support area of the hydraulic support may lead to insufficient caving of the uncaving top coal and the direct roof due to the small span of the suspended roof. Therefore, based on the stopping caving distance of 26 m, a stopping caving coefficient K is multiplied, and finally, the final stopping caving distance is calculated by theoretical analysis to meet Formula (2):

$$L_f = L_C \times K \quad (2)$$

In this context, L_f is the final stopping coal caving distance; L_C is the stopping coal caving distance, 26 m; K stopping caving coal caving coefficient, 1.15.

The final stopping coal caving distance L_f = 29.9 m is obtained; therefore, the final stopping coal caving distance L_C of the 8309 extra-thick fully mechanized caving face is 30 m.

3.2.2. Stability Analysis of Key Blocks of Not Stopping Coal Caving

The mechanical model of the stability of the key block in the case of whether the withdrawal space of the final mining stage stops coal drawing is shown in Figure 5. Within the figure, q_s is the support force of stopping coal pillar; q_z is the support force of the hydraulic support; the horizontal thrust T and shear force Q_g are generated by the action of A in front of the working face; and q_A and q_B are the load of the fractured rock block above A and B; G is the gravity of B itself.

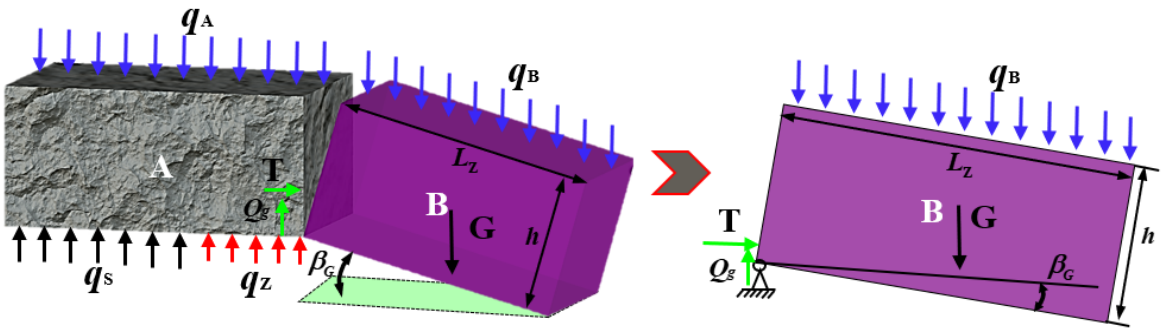


Figure 5. Mechanical model of key block stability under the condition of whether to stop coal caving or not. The B rock block is the key research block in this paper, and the stability of the B rock block is related to the stability of the surrounding rock in the underlying withdrawal space. Therefore, the B rock block is highlighted and changed to magenta.

In the final mining stage, the coal is not stopped, and there is still a large gap between the goaf and the main roof. The main roof is broken, the B activation and rotation space is large, and the B rotation angle becomes larger. According to the "masonry beam" structure "S-R" stability theory, it is judged whether the hinged structure of the key block is stable or not when the final mining is not stopped.

In the final mining stage, the coal caving is not stopped, the working face is normally mined 19.0 m, and only 7.7 m is directly filled in the goaf. According to the calculation formula of the rotation angle of B,

$$\beta_G = \arcsin\frac{h_j - (\sum h_s(K_{ps} - 1) + h_2(K_{P2} - 1))}{L_Z} \tag{3}$$

where β_G is the rotation angle of B; L_{GZ} is the fracture length of B along the strike of the working face, which is similar to 26 m; h_j is the mining height of the coal seam, 19.0 m; $\sum h_s$ is the thickness of the rock between the main roof and the coal seam, 7.7 m; K_{ps} is the average residual bulking coefficient of direct roof strata, 1.15; h_2 is the height of the uncaving top coal, 0 m; K_{p2} is the average residual bulking coefficient of the uncaving top coal, 1.05.

In the case of not stopping the top coal, the rotation angle of B is 43°.

The key block that does not experience slip instability must satisfy Formula (4); Formula (4) further refines and derives the final judgment Formula (5) of slip instability [31]:

$$T\mathrm{tg}\varphi < Qg \tag{4}$$

$$h + h_1 \leqslant \frac{\sigma_c}{30\gamma}\left(\mathrm{tg}\varphi + \frac{3}{4}\sin\beta_G\right)^2 \tag{5}$$

In this context, T is the horizontal thrust of B; tgφ is the friction coefficient between rock blocks, taken as 0.6; Q_g is the shear force of B; h is the thickness of key block B, 14.1 m; h_1 is the thickness of the B load rock layer, 19.4 m; φ_c is the ultimate compressive strength of B, 86 MPa; γ is the average bulk density of the overlying rock, 0.025 MN.

The key block that does not experience rotary deformation instability must meet Formulas (6) and (7):

$$T > s\eta\sigma_c \tag{6}$$

$$h + h_1 \leqslant \frac{\sigma_c}{30\gamma}\left(\mathrm{tg}\varphi + \frac{3}{4}\sin\beta_G\right)^2 \tag{7}$$

In this context, s is the contact surface area of B and C_1; $\eta\sigma_c$ is the extrusion strength of B at the corner; i is B fracture degree; l is assumed to be equal to L_Z, 26 m.

Under the condition of not stopping coal caving, the key block "summary of S-R stability theory analysis parameters" is shown in Table 1. The results show that under the condition of not stopping coal caving, there will be no sliding instability between the key blocks of the basic roof, and because the B rotation angle is too large, there may be rotational deformation instability.

Table 1. Summary of theoretical analysis parameters of "S-R" stability of key blocks without stopping coal caving.

Summary of Theoretical Analysis Parameters of "S-R" Stability of Key Blocks Without Stopping Coal Caving	
B rotation angle β_G	43°
$\frac{\sigma_c}{30\gamma}\left(\mathrm{tg}\varphi + \frac{3}{4}\sin\beta_G\right)^2 > h + h_1$	141.6 > 33.5
$\frac{0.15\sigma_c}{\gamma}\left(i^2 - \frac{3}{2}i\sin\beta_G + \frac{1}{2}\sin^2\beta_G\right) < h + h_1$	−14.6 < 33.5 (rotary deformation instability)

3.2.3. Stability Analysis of Key Blocks for Stopping Coal Caving

In the final mining stage, coal caving is stopped, and only 3.5 m of coal is mined in the working face. The rest of the uncaving top coal is fully filled with the goaf with the direct roof caving. According to the above B rotation angle calculation Formula (3), the following can be obtained:

In the case of stopping the top coal, β_G is 3.5°;

h_j is the mining height of the coal seam, 3.5 m; h_2 is the height of the uncaving top coal, 15.5 m.

The key block does that not experience slip instability must meet Formula (5), and the key block that does not experience rotate deformation instability must meet Formula (7). Under the condition of reasonable stopping coal caving, the key block "S-R" stability theory analysis parameter summary is shown in Table 2. The results show that under the condition of reasonable stopping coal caving, there will be no sliding instability between the key blocks of the main roof and there will be no rotary deformation instability.

Table 2. Summary of theoretical analysis parameters of "S-R" stability of key blocks with stopping coal caving.

Summary of Theoretical Analysis Parameters of "S-R" Stability of Key Blocks with Stopping Coal Caving	
B rotation angle β_G	3.5°
$\frac{\sigma_c}{30\gamma}\left(\mathrm{tg}\varphi + \frac{3}{4}\sin\beta_G\right)^2 > h + h_1$	47.8 > 33.5
$\frac{0.15\sigma_c}{\gamma}\left(i^2 - \frac{3}{2}i\sin\beta_G + \frac{1}{2}\sin^2\beta_G\right) > h + h_1$	126.0 < 33.5

According to the results of the stability of the key block in whether to stop the coal caving or not, with the continuous advancement of the final mining face, the goaf below B is filled by the non-caving coal and the direct roof caving, the rotation space and rotation angle

of B fracture are reduced, and the probability of slip instability and rotation deformation instability between key blocks decreases.

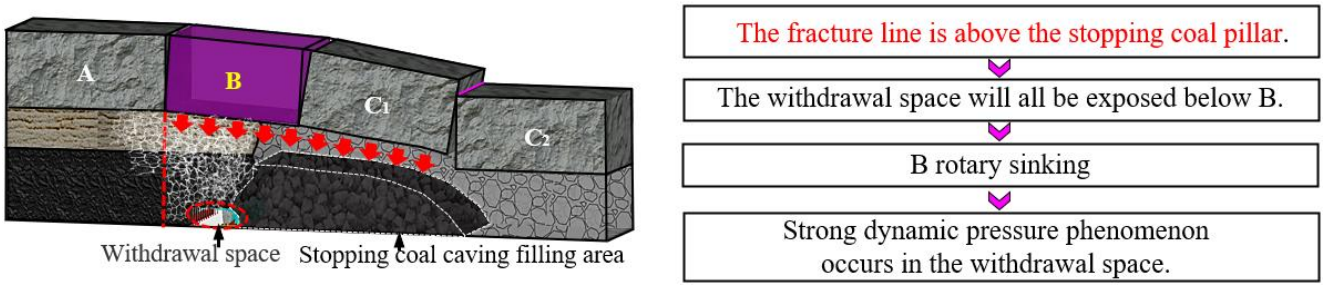
3.3. The Relative Space–Time Layout of the Main Roof Fracture Position and the Withdrawal Space

The influence of different fracture positions of the final mining main roof on the underlying withdrawal space disturbance is significantly different. The relative space–time layout of the main roof fracture position and the withdrawal space can be roughly divided into three categories: the first case—the fracture position is above the stopping coal pillar; the second case—the fracture position is above the withdrawal space; the third case—the fracture position is above the goaf.

(1) During the whole mining period, the "masonry beam" structure is always in a dynamic equilibrium state. In the early stage of the next stage of pressure, the fracture position of the main roof will first fracture above the stopping coal pillar (Figure 6a), and the coal wall of the stopping coal pillar becomes an important fulcrum for the stable migration of the "masonry beam" structure. The withdrawal space is arranged in the coal body behind the fracture line. At this time, the withdrawal space will be all exposed below the unstable B region. The B rotary sinking leads to the strong dynamic pressure phenomenon in the withdrawal space. The roof of the support area of the hydraulic support is cut off in a large area due to a lack of support, which leads to the subsequent hydraulic support being crushed and unable to withdraw. This arrangement is the most unfavorable for the work of stopping mining and removing the support;

(2) If the withdrawal space is arranged below the fracture line of the main roof (Figure 6b), the overlap width between B and the solid coal decreases, which increases the possibility of the sliding instability of B. During the withdrawal of the support, the rotation and subsidence of B lead to the risk of roof cutting and support crushing in the withdrawal space;

(3) If the fracture position of the basic roof is located above the goaf (Figure 6c), most of the dynamic and static load stresses of B rotary sinking act on the stopping coal caving filling area, which greatly reduces the damage of B rotary sinking to the complete A above the stop coal pillar. The withdrawal space is arranged under the A region. This arrangement is most beneficial to the stop mining and withdrawal work. The relative space–time layout of the basic roof fracture position and the withdrawal space is shown in Figure 6.



(**a**)

Figure 6. *Cont.*

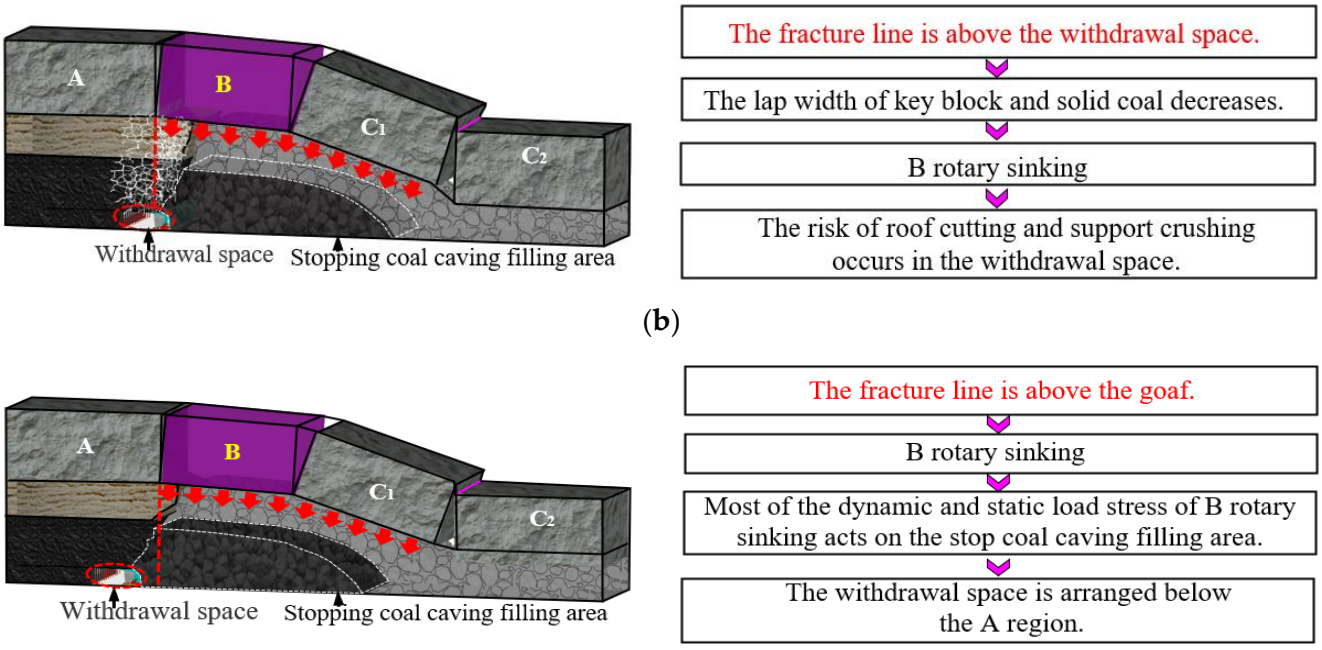


Figure 6. The relative space–time layout of main roof fracture position and withdrawal space: (**a**) The fracture position is located above the stopping coal pillar; (**b**) the fracture position is located above the withdrawal space; (**c**) the fracture position is located above the goaf. The magenta straight line in the figure indicates the position where the two rock blocks are squeezed each other when the steps of the two rock blocks collapse when is not stop coal caving in this interval. The text mark red is to facilitate the reader to accurately grasp the characteristics of this paper. One of the major research features is the spatial and temporal relationship between the different fracture positions of the three basic roofs and the underlying withdrawal space.

4. Simulation Analysis on Stability of the Withdrawal Space in the Final Mining Stage

4.1. Numerical Model Establishment of the Withdrawal Space in the Final Mining Stage

According to the actual geological conditions of the 8309 extra-thick fully mechanized caving face and the mechanical parameters of the coal and rock strata (Table 3), the UDEC numerical analysis model is constructed as shown in Figure 7. The UDEC simulation software was used to construct a model with a length × width of 300 m × 112.3 m to simulate the spatial stress evolution law and overburden structure characteristics of large-section withdrawal under different stopping coal caving distances and different fracture positions of the main roof. The model is externally imported into a 3.5 m hydraulic support for simulating real top coal mining. The left, right, and lower boundaries of the model limit the speed and displacement. The upper boundary applies a 12.0 MPa uniform load and increases according to the buried depth gradient. The lateral pressure coefficient is set to 1.2.

Table 3. Correction parameters of model.

Rock Stratum	Bulk Modulus (GPa)	Shear Modulus (GPa)	Cohesion (MPa)	Angle of Internal Friction (°)	Tensile Strength (MPa)
Medium sandstone	10.06	6.62	2.37	43.7	0.36
Sandy mudstone	2.59	1.86	0.84	24.0	0.08
3~5# extra-thick coal seam	1.70	0.88	0.53	17.5	0.02
Mudstone	2.93	2.20	0.97	26.6	0.09
Grit stone	4.61	3.46	1.60	38.1	0.09

Table 3. *Cont.*

Rock Stratum	Bulk Modulus (GPa)	Shear Modulus (GPa)	Cohesion (MPa)	Angle of Internal Friction (°)	Tensile Strength (MPa)
Fine sandstone	10.51	6.92	2.36	43.4	0.37
Sandy mudstone	2.41	1.73	1.19	32.4	0.03
Grit stone	12.34	8.13	2.65	44.9	0.49
Sandy mudstone	2.41	1.73	1.19	32.4	0.03
Mudstone	2.68	2.12	0.95	26.4	0.09
Grit stone	10.11	7.59	2.55	44.6	0.45

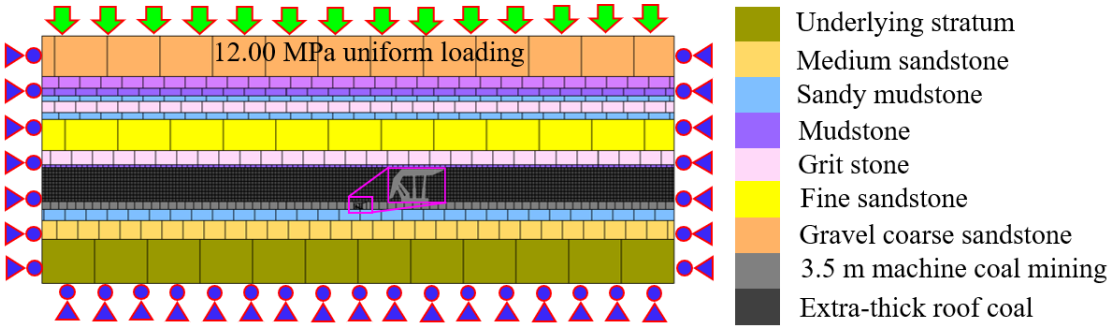


Figure 7. Numerical analysis model of extra-thick comprehensive caving working face. The dark blue hinge support in the diagram represents the velocity and displacement of the left, right and lower boundaries of the constraint model; the light green down arrow indicates that a uniform load of 12.0 MPa is applied to the model.

4.2. Study on the Stability of the Withdrawal Space under Different Stopping Coal Caving Distances

A reasonable stopping coal caving distance is related to the stable migration of overlying strata in the final mining face and the withdrawal space. In this section, it is proposed to analyze the migration characteristics and stress evolution law of overburden structures in withdrawal space under different stopping coal caving distances of 0 m, 10 m, 20 m, 30 m, 40 m, and 50 m. For the convenience of expression, L_C is used to represent the stopping coal caving distance.

4.2.1. Migration Characteristics of the Overlying Rock Structure in the Final Mining Withdrawal Space

The migration characteristics of the overlying strata structure in the withdrawal space under different stopping coal caving distances are shown in Figure 8. From Figure 8, it can be seen that with the increase in the distance of stopping coal caving, the number and range of key blocks undertaken by top coal caving increase, and the rotation angle of the key blocks slows down.

(1) When L_C = 0 m (Figure 8a), due to the large mining space, there is a large range of suspended roof area under B, C_1 compacts the gangue, and the vertical drop between B and C_1 is large. Only when B rotates and sinks at a large angle can it be hinged with C_1. At this time, the dynamic and static load stress generated by B rotation is concentrated on the overburden rock in the withdrawal space due to the large rotation angle of B, and the extrusion deformation in the withdrawal space is serious, resulting in a crushing accident.

(2) When L_C = 10 m and 20 m (Figure 8b,c), part of the goaf below B is filled with unplaced top coal. The rotation angle of B is slower than that of not stopping coal caving. There are still some suspended roof areas below B and the rotation of B is blocked. The vertical drop between B and C_1 increases, especially when L_C = 20 m. The large drop

means that the interaction force between C_1 and B is limited. Most of the dynamic and static loads generated by B rotation act on the stopping coal pillar and the stopping coal caving filling area within a limited range. The overburden rock in the withdrawal space is still subjected to concentrated load. Especially when L_C = 10 m, the extrusion deformation in the withdrawal space is serious, and there is a risk of support crushing in the support area of the hydraulic support.

(3) When L_C = 30 m and 40 m (Figure 8d,e), the goafs of B and C_1 are filled with unplaced top coal. B and C_1 are buffered and supported by the uncaving top coal, and the rotation angle of B is greatly slowed down. During the rotation and subsidence of B, it is supported by the full range of top coal caving, stopping coal pillars, and C_1. At the same time, C_1 is affected by the rear C_2 interaction. Therefore, at this time, the key blocks are interlocked and interacted to form a stable hinged structure. The top coal caving filling area bears most of the concentrated load of B, and the overburden rock in the withdrawal space is less affected by the load disturbance. There is no obvious deformation in the withdrawal space, and there will be no support crushing accident in the support area of the hydraulic support. The spatial section of the withdrawal channel area meets the withdrawal requirements.

(4) When L_C = 50 m (Figure 8f), the unplaced top coal fills the goaf of B, C_1, and C_2, the rotation angle of B is further reduced, and the stable hinged structure is formed by the support of the uncaving top coal, the stopping coal pillar, and C_1 and C_2 during the rotation and subsidence of B. However, compared with L_C = 30 m, the difference in withdrawal space deformation is small. It can be seen that when L_C > 30 m, the increase in stopping coal caving distance has no obvious effect on the protection and gain of withdrawal space, which invalidly increases the stopping coal caving distance and seriously wastes coal resources.

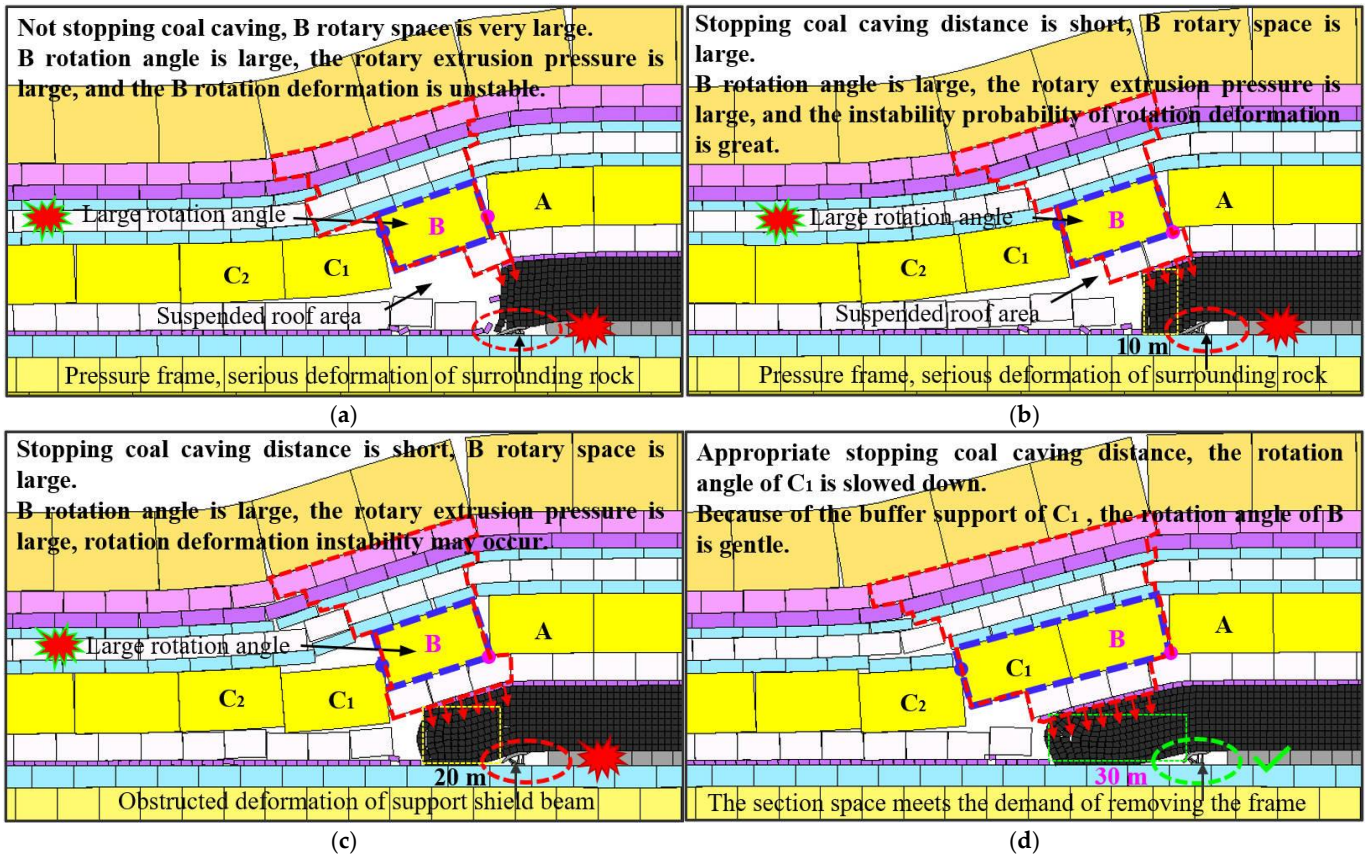
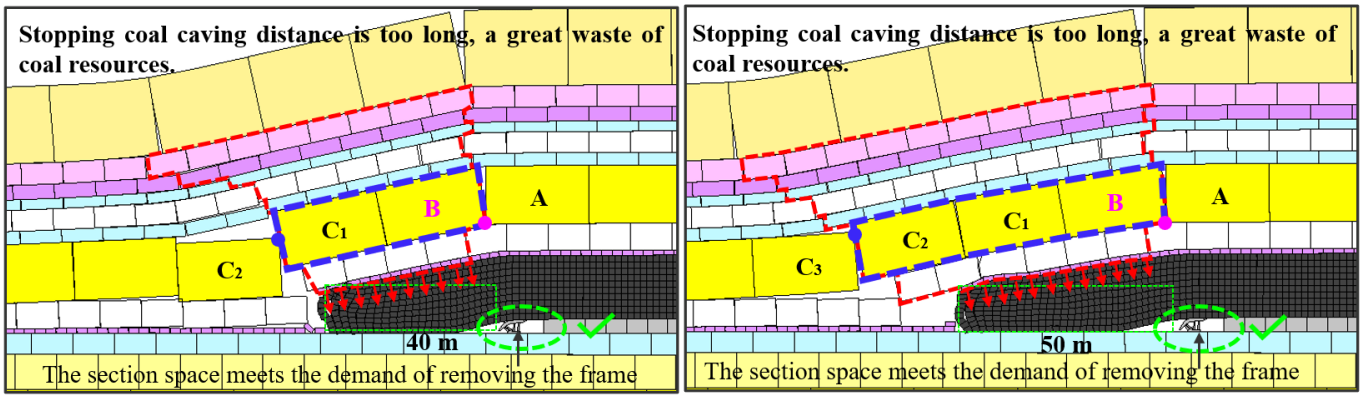


Figure 8. *Cont.*

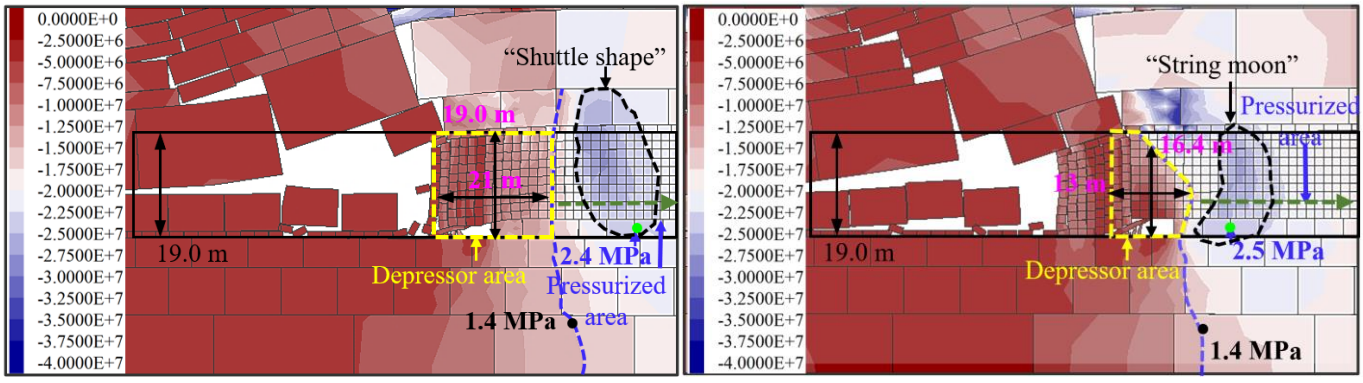


(**e**) (**f**)

Figure 8. The migration characteristics of the overlying rock structure in the withdrawal space under different stopping coal caving distances: (**a**) L_C = 0 m; (**b**) L_C = 10 m; (**c**) L_C = 20 m; (**d**) L_C = 30 m; (**e**) L_C = 40 m; (**f**) L_C = 50 m.

4.2.2. Evolution Law of Vertical Stress in the Final Mining Withdrawal Space

The evolution law of vertical stress in the withdrawal space under different stopping coal caving distances is shown in Figure 9. In order to facilitate the analysis and comparison, the original rock stress of the coal seam where the withdrawal space is located is marked in the diagram. Taking the boundary between the goaf and the withdrawal space as the starting line, the withdrawal space, and the stopping coal pillar in front of it are divided into a depressor area and pressurized area along the direction of the stopping coal pillar. The vertical stress distribution is introduced into the following evaluation and analysis indicators: The lateral extension range D_i of the depressor area in the withdrawal space. Due to the fact that there is little difference in the degree of coal plasticization at the edge of the support area of the hydraulic support under different stopping coal caving distances during the rotation and sinking of B, in order to intuitively and fairly reflect the influence of the change in stopping coal caving distance on the longitudinal extension range of the depressor area of withdrawal space, D_o is used to represent the longitudinal extension range of the depressor area of the withdrawal channel. The peak stress σ_w of the middle coal body in front of the withdrawal space: $[(D_i(L_C) - D_i(L_C = 0))/D_i(L_C = 0)] \times 100\%$ (the percentage of the difference between $D_i(L_C)$ and $D_i(L_C = 0)$ in the withdrawal space at different stopping distances); $[(D_o(L_C) - D_o(L_C = 0))/D_o(L_C = 0)] \times 100\%$ (percentage of difference between $D_o(L_C)$ and $D_o(L_C = 0)$ at different stopping coal caving distances); $\sigma_w(L_C)/\sigma_w(L_C = 0)$ (under different stopping coal caving distances, the increase coefficient of the peak stress in front of the withdrawal space).



(**a**) (**b**)

Figure 9. *Cont.*

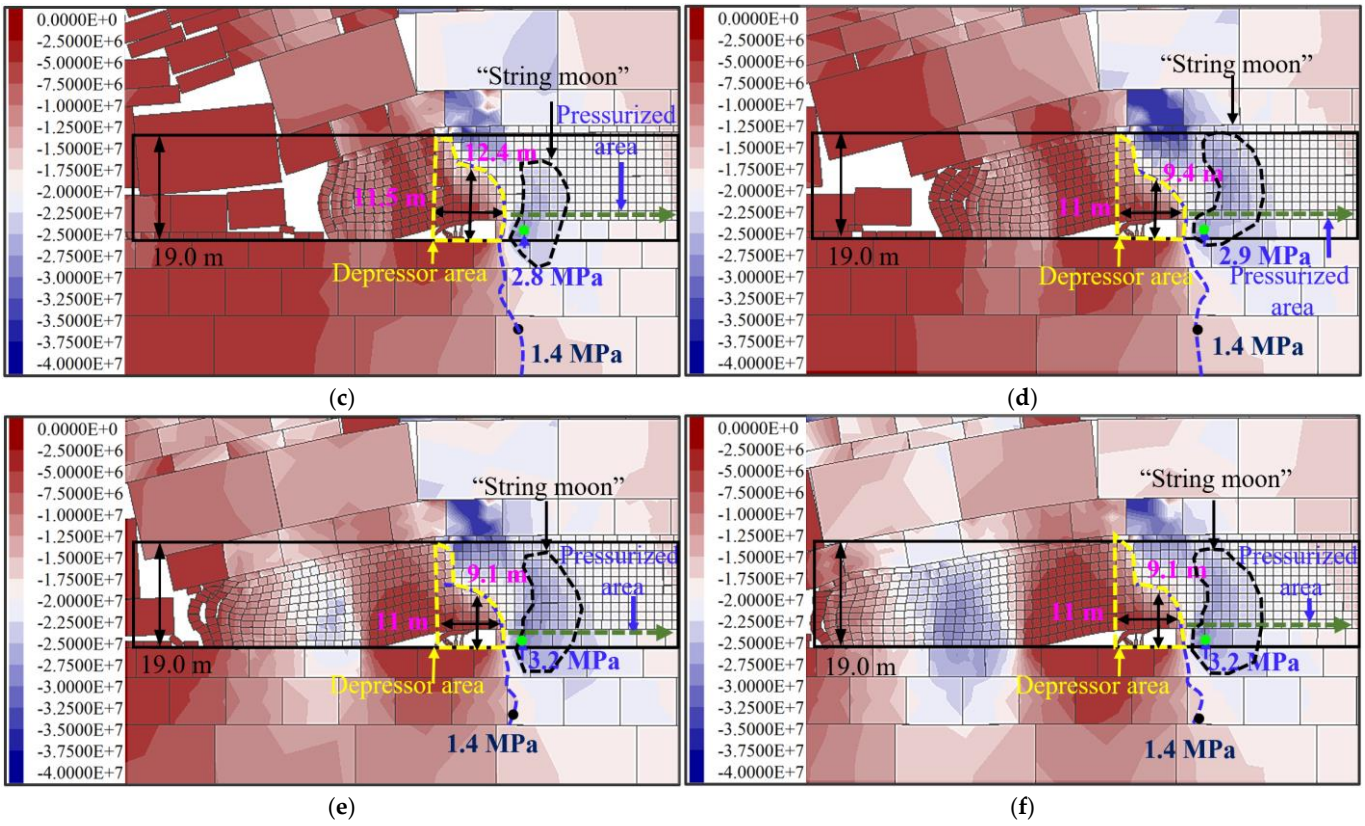


Figure 9. The evolution law of vertical stress in withdrawal space under different stopping coal caving distances: (**a**) L_C = 0 m; (**b**) L_C = 10 m; (**c**) L_C = 20 m; (**d**) L_C = 30 m; (**e**) L_C = 40 m; (**f**) L_C = 50 m.

(1) When L_C = 0 m (Figure 9a), the overlying top coal and pseudo-top of the withdrawal space are all located in the depressor area, D_i is 21 m, D_o is 20.4 m. A "shuttle shape" stress-focused area is formed in front of the stopping coal pillar, and σ_w is 2.4 MPa. Due to the large plasticizing area in front of the withdrawal space, σ_w is far away from the coal wall in front of the withdrawal space.

(2) When L_C = 10 m (Figure 9b), the top coal and its direct roof in the support area of the hydraulic support are all located in the depressor area, and the depressor area in front of the withdrawal space and the stopping coal pillar is reduced, D_i is 13 m, D_o is 16.4 m. A "string moon"-type stress-focused area is formed in front of the coal pillar, and σ_w is 2.5 MPa. Due to the decrease in the plasticizing area in front of the withdrawal space, σ_w is close to the coal wall in front of the withdrawal space.

(3) When L_C = 20 m (Figure 9c), the range of the depressor area in front of the withdrawal space and stopping coal pillar is further reduced, D_i is 11.5 m and D_o is 12.4 m. A "string moon" stress-focused area is formed in front of the stopping coal pillar, and σ_w is 2.8 MPa. σ_w is closer to the coal wall in front of the withdrawal space than L_C = 0 m.

(4) When L_C = 30 m (Figure 9d), the range of the depressor area in front of the withdrawal space and stopping coal pillar is greatly reduced, D_i is 11 m, D_o is 9.4 m. A "string moon" stress-focused area is formed in front of the stopping coal pillar, and σ_w is 2.9 MPa. σ_w is much closer to the coal wall in front of the withdrawal space than L_C = 0 m.

(5) When L_C = 40, 50 m (Figure 9e,f), the range of the depressor area in front of the withdrawal space and stopping coal pillar are greatly reduced, D_i is 11 m, D_o is 9.1 m. A "string moon" stress-focused area is formed in front of the stopping coal pillar, and σ_w is 3.2 MPa. σ_w is much closer to the coal wall in front of the withdrawal space than L_C = 0 m.

(6) Under different stopping coal caving distances, $[(D_i(L_C) - D_i(L_C = 0))/D_i(L_C = 0)] \times 100\%$ is −38.1%, −45.2%, −47.6%, −47.6%, −47.6%, respectively, compared with

L_C = 0 m. When L_C = 30 m, D_i reaches the minimum value, which is about 47.6% lower than that of L_C = 0 m. $[(D_o(L_C)–D_o(L_C = 0))/D_o(L_C = 0)]\times100\%$ is −19.6%, −39.2%, −53.9%, −55.4%, −55.4%, respectively, compared with L_C = 0 m. When L_C = 40 m, D_o reaches the minimum value, which is about 55.4% lower than of L_C = 0 m but the decrease is not obvious compared with L_C = 30 m.

(7) Under different stopping coal caving distances, $\sigma_w(L_C)/\sigma_w(L_C = 0)$ is 1.04, 1.17, 1.21, 1.33, and 1.33, respectively, compared with L_C = 0 m. The increase in σ_w is smaller than that of L_C = 0 m. When L_C = 30 m, the increase coefficient of vertical stress peak is only 1.21.

(8) Through the analysis of quantitative results, it can be seen that the increase in stopping coal caving distance has little influence on the peak stress in front of stopping coal pillar, and has significant influence on the range of the depressor area of surrounding rock in the withdrawal space. The increase in the stopping coal caving distance can reduce the horizontal and vertical extension range of the depressor area in the withdrawal space. At the same time, the plasticization range of the coal body and the direct roof in front of the stopping coal pillar is reduced, and the integrity is enhanced, which is beneficial to control the internal extrusion deformation of the coal wall of the stopping coal pillar.

Therefore, according to the vertical stress evolution law of different stopping caving distances, the stopping caving distance L_C is selected as 30 m.

4.2.3. Evolution Law of Maximum Shear Stress in the Final Mining Withdrawal Space

The maximum shear stress can characterize the deformation and failure of coal and rock mass under the combined action of complex stress. In this paper, the maximum shear stress index is introduced to study the complex stress environment and deformation and failure mechanism of surrounding rock in the large-section withdrawal space under different stopping caving distances. The evolution law of maximum shear stress of overlying rock in the withdrawal space under different stopping caving distances is shown in Figure 10. The evolution of the maximum shear stress is introduced into the following evaluation indexes: the maximum shear stress peak τ_w of the middle coal in front of the retreat space; τ_w from the withdrawal space coal wall distance D_w; $[(\tau_w(L_C) - \tau_w(L_C = 0))/\tau_w(L_C = 0)] \times 100\%$ (the percentage of the peak difference between $\tau_w(L_C)$ and $\tau_w(L_C = 0)$ in front of the withdrawal space under different stopping coal caving distances.); $[(D_w(L_C) - D_w(L_C = 0))/D_w(L_C = 0)] \times 100\%$ (the percentage of the range difference between the withdrawal space $D_w(L_C)$ and $D_w(L_C = 0)$ under different stopping distances).

(1) It can be seen from Figure 10 that with the increase in the stopping coal caving distance (L_C), the range of maximum shear stress low-value area of surrounding rock in withdrawal space is shrinking, and the range of the maximum shear stress increase area is expanding. The range of stress increase area first extends longitudinally to the direction of the withdrawal space (0 m→20 m), and then extends laterally to the depth of the stopping coal pillar (20 m→30 m). When $L_C \geq 30$ m, there is no obvious expansion of the stress increase area (30 m→50 m).

(2) The maximum shear stress peak τ_w of the central coal in front of the withdrawal space at different stopping caving distances is 1.48 MPa, 1.52 MPa, 1.70 MPa, 1.82 MPa, 2.01 MPa, and 1.96 MPa, respectively. The percentage of the difference between the peak values of τ_w (L_C) and τ_w (L_C = 0) $[(\tau_w(L_C) - \tau_w(L_C = 0))/\tau_w(L_C = 0)] \times 100\%$ in the central coal in front of the withdrawal space is 2.70%, 14.86%, 22.97%, 35.81%, and 32.43%, respectively. When L_C = 40 m, the maximum shear stress peak τ_w of the middle coal body in front of the withdrawal space reaches the maximum value of 2.01 MPa, which is 35.81% higher than that of L_C = 0 m.

(3) The distance D_w between τ_w and the coal wall in the withdrawal space is 27 m, 12.5 m, 6 m, 5 m, and 5 m, respectively, under different stopping coal caving distances. The percentage of the range difference between the withdrawal space $D_w(L_C)$ and

$D_w(L_C = 0)$ $[(D_w(L_C) - D_w(L_C = 0))/D_w(L_C = 0)] \times 100\%$ is −53.7%, −77.8%, −81.5%, −81.5%, and −81.5%, respectively. When L_C = 30 m, the distance between τ_w and the coal wall in the withdrawal space D_w reaches the minimum value of 5 m, which is 81.5% less than that of L_C = 0 m.

(4) Through the analysis of quantitative results, it can be seen that with the increase in stopping coal caving distance, the maximum shear stress peak of the middle coal body in front of the withdrawal space is greatly transferred to the shallow coal body of the stopping coal pillar. When the maximum shear stress peak area of L_C = 0 m is far away from the shallow coal body and the peak value is small, it shows that the stopping coal caving operation leads to the large-scale plasticization of the stopping coal pillar, the coal body integrity is poor, the strength is low, and the shallow coal body does not have good bearing and shear resistance. When the maximum shear stress increase area of L_C = 30 m is close to the shallow coal body of the stopping coal pillar to the greatest extent, it shows that the shallow coal body of the stopping coal pillar is greatly weakened by the mining disturbance of the working face, the solid coal remains in a good and complete state, and the shallow coal body of the stopping coal pillar in the final mining stage has good bearing and shear performance.

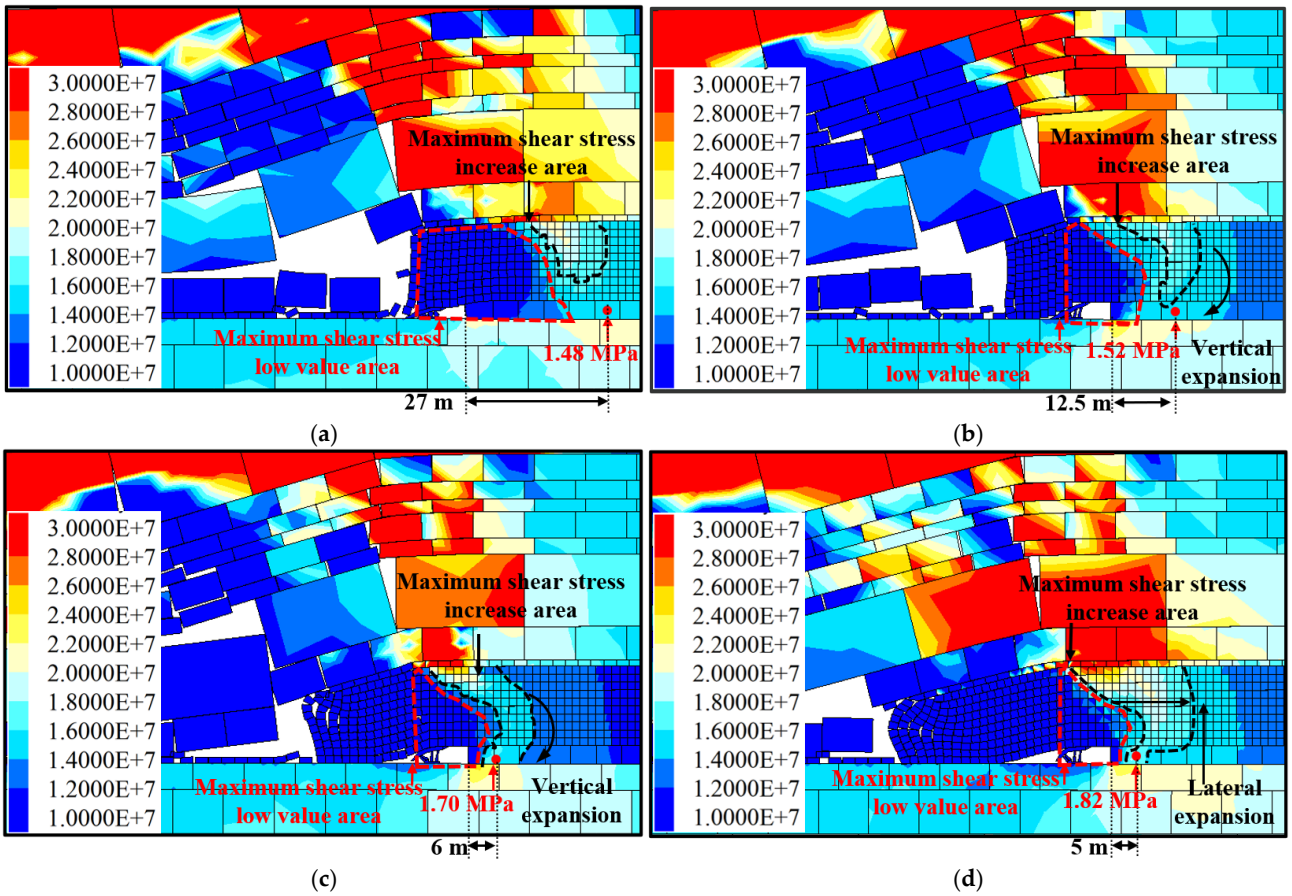


Figure 10. *Cont.*

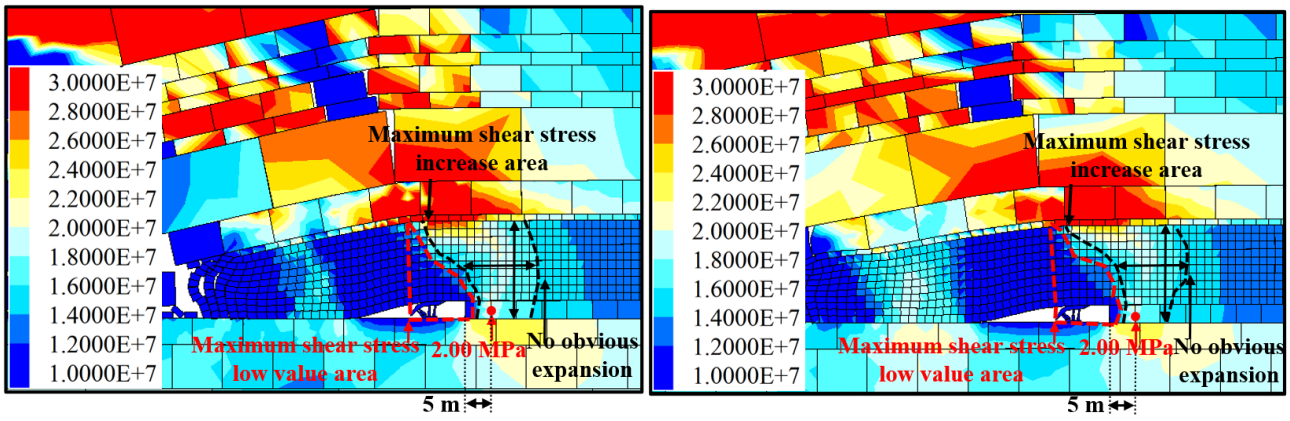


Figure 10. The evolution law of maximum shear stress in withdrawal space under different stopping coal caving distances: (**a**) L_C = 0 m; (**b**) L_C = 10 m; (**c**) L_C = 20 m; (**d**) L_C = 30 m; (**e**) L_C = 40 m; (**f**) L_C = 50 m. In the figure, the red dotted line delineates the low value area of the maximum shear stress, and the black dotted line delineates the high value area of the maximum shear stress. In order to facilitate readers to read, the corresponding line color indicates the regional characteristics.

Therefore, according to the maximum shear stress evolution law of different stopping coal caving distances, the stopping coal caving distance L_C is selected as 30 m.

4.3. Study on the Stability of the Withdrawal Space under Different Fracture Positions of the Main Roof

4.3.1. Migration Characteristics of the Overlying Rock Structure in the Withdrawal Space Under Different Fracture Positions of the Main Roof

The distance of stopping coal caving at the end of mining is 30 m, and the structural characteristics of overlying strata in the withdrawal space under different fracture positions are shown in Figure 11. With the continuous advancement of the working face, the influence of different fracture positions on the deformation of the withdrawal space is significant.

(1) When the fracture position is located above the stopping coal pillar (Figure 11a), the dynamic and static loads of the rotary sinking parts of B and C_1 are concentrated on the upper part of the whole withdrawal space, and the plasticizing damage of the shallow coal body of the stopping coal pillar is serious, which leads to the serious extrusion deformation in the section of the withdrawal space; consequently, the support crushing accident occurs in the support area of the support, and the section space of the withdrawal channel area cannot withdraw the support normally.

(2) When the fracture position is located above the withdrawal space (Figure 11b), the dynamic and static loads of the B and C_1 rotary sinking parts are concentrated above the partial withdrawal space. Compared with Figure 11a, it is found that the deformation of the support area of the hydraulic support is more serious, and the roof of the area is completely crushed but the section of the withdrawal channel area is relatively complete.

(3) When the fracture position is located above the goaf (Figure 11c), the dynamic and static loads of B and C_1 rotary subsidence are concentrated on the stopping coal caving filling area behind the support, and the withdrawal space is placed under the stable A region. The overall section control effect of the withdrawal space is good. This arrangement is conducive to the safe and efficient withdrawal of the final mining.

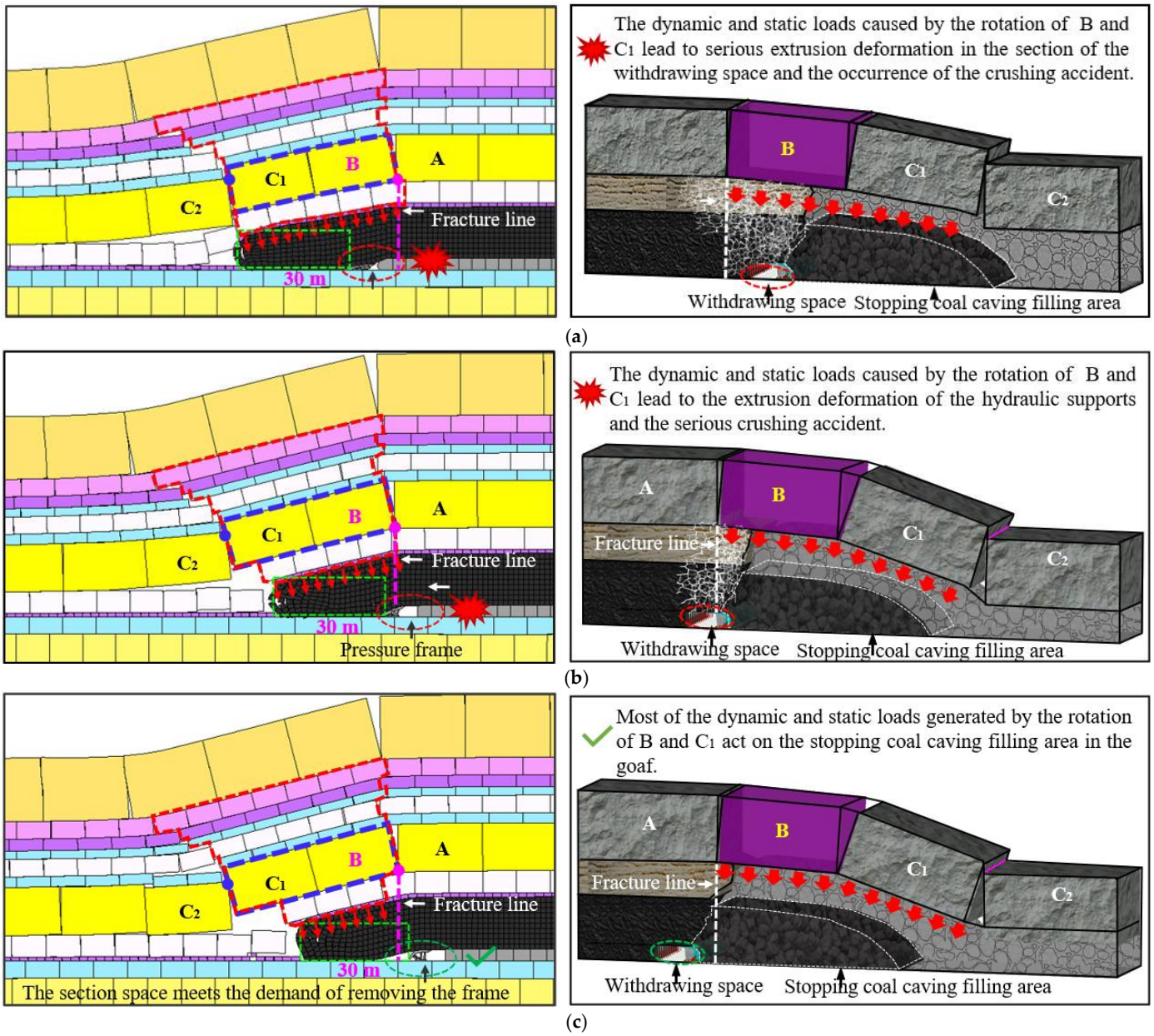


Figure 11. The structural characteristics of overlying strata in the withdrawal space under different fracture positions: (**a**) the fracture position is located above the stopping coal pillar; (**b**) the fracture position is located above the withdrawal space; (**c**) the fracture position is located above the goaf. The blue dotted line on the left side of the figure delineates the buffer support range of the stopping coal caving area to the overlying key rock blocks. The red dotted line and the downward arrow indicate the dynamic and static load disturbance of the unstable rock strata in the rear of the goaf on the underlying stopping coal caving area. The red explosion shape indicates the serious mine pressure disaster in the underlying area under the influence of different fracture positions. The arrows and related marks in the right sketch correspond to the information in the left sketch.

4.3.2. Evolution Characteristics of Vertical Stress and Maximum Shear Stress of Overlying Strata in the Withdrawal Space under Different Fracture Positions of the Main Roof

The evolution law of vertical stress and maximum shear stress of overlying strata in the withdrawal space under different fracture positions of the main roof is shown in Figure 12. The evolution analysis of vertical stress and maximum shear stress also introduces the above evaluation and analysis indexes.

When the fracture position is located above the stopping coal pillar (Figure 12a), in terms of vertical stress, the overlying top coal and direct roof of the withdrawal space are almost all located in the depressor area, D_i is 19 m and D_o is 26.7 m. A "Carillon shape" stress-focused area is formed in front of the stopping coal pillar, and σ_w is 2.3 MPa. Due to the large plasticized area in front of the withdrawal space, σ_w is far away from the coal wall in front of the withdrawal space. In terms of maximum shear stress, the large-scale coal body in the shallow part of the stopping coal pillar is in the low-value area of maximum shear stress.

(1) When the fracture position is located above the withdrawal space (Figure 12b), in terms of vertical stress, the depressor area in front of the stopping coal pillar is greatly reduced and the depressor area above the withdrawal space is reduced to a certain extent, D_i is 12 m and D_o is 10.4 m. A "string moon" stress-focused area is formed in front of the stopping coal pillar, and σ_w is 2.8 MPa, which is close to the coal wall when the fracture position is located above the stopping coal pillar. In terms of maximum shear stress, the maximum shear stress peak τ_w of the middle coal body in front of the withdrawal space is 1.7 MPa, and the distance between τ_w and the coal wall in the withdrawal space D_w is 6 m.

(2) When the fracture position is located above the goaf (Figure 12c), in terms of vertical stress, the depressor area in front of the withdrawal space and the stopping coal pillar is greatly reduced, D_i is 11 m and D_o is 9.4 m. A "string moon" stress-focused area is formed in front of the stopping coal pillar, and σ_w is 2.9 MPa. In terms of maximum shear stress, the maximum shear stress peak τ_w of the middle coal body in front of the withdrawal space is 1.82 MPa, and the distance between τ_w and the coal wall in the withdrawal space D_w is 5 m.

(3) Through the analysis of quantitative results, in terms of vertical stress, when the fracture position is above the goaf, the transverse and longitudinal range of the depressor area is the smallest, and D_i and D_o are 42.1% and 64.8% lower than those when the fracture position is above the stopping coal pillar, respectively. In terms of maximum shear stress, when the fracture position is located above the goaf, the maximum shear stress peak is the closest to the coal wall in the withdrawal space, and D_w is 5 m. When the fracture position is located above the stopping coal pillar, the stopping coal pillar is plasticized in a large range, the integrity of the coal body is poor, and the shallow coal body does not have good bearing and shear performance. When the fracture position is located above the withdrawal space, the plasticization range of the stopping coal pillar area is greatly reduced but the top coal and direct top plasticization above the withdrawal space is serious, the coal body integrity is poor, and the top coal does not have good bearing and shear performance; in contrast, when the fracture position is located above the goaf, the top coal above the stopping coal pillar and withdrawal space is greatly weakened by the mining disturbance of the working face. The surrounding rock integrity of the withdrawal space is good, and the coal and rock mass of the withdrawal space in the final mining stage has good bearing and shear resistance.

In summary, the main roof fracture position is located above the goaf, and the withdrawal space is arranged under the A region. This arrangement form is most beneficial to the stop mining and withdrawal work.

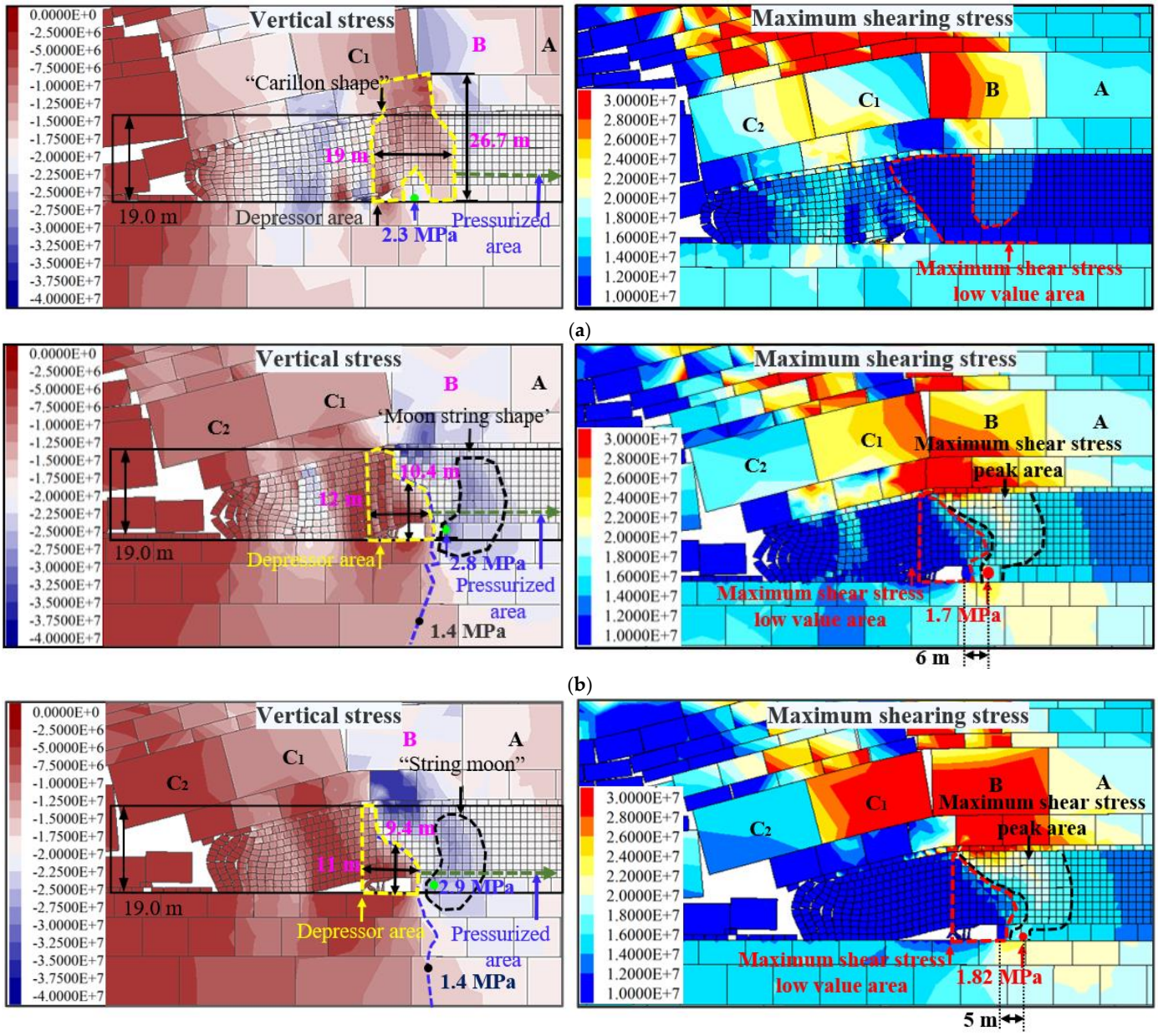


Figure 12. The evolution characteristics of vertical stress and maximum shear stress in withdrawal space under different fracture positions: (**a**) the fracture position is located above the stopping coal pillar; (**b**) the fracture position is located above the withdrawal space; (**c**) the fracture position is located above the goaf. In the left figure, the yellow dotted line delineates the vertical stress depressor area, the black dotted line delineates the vertical stress pressurized area, the red dotted line in the right figure delineates the maximum shear stress low value area, the black dotted line delineates the maximum shear stress peak area, and uses the same color font color to describe the feature area.

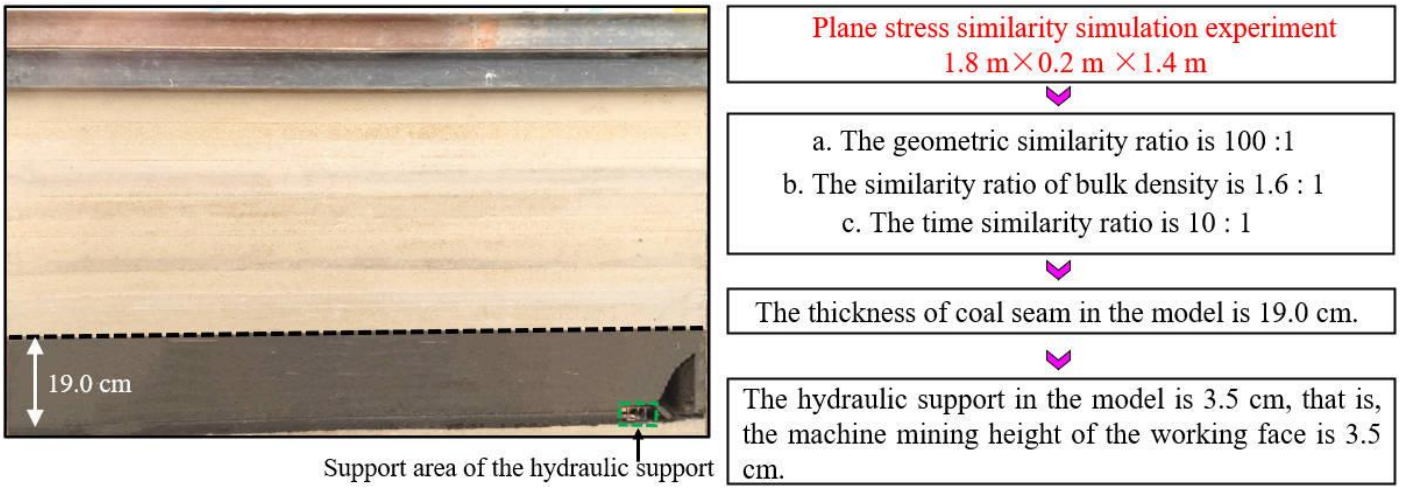
4.4. Physical Similarity Simulation Analysis of Stopping Coal Caving Operations in the Withdrawal Space of the Final Mining Stage

In order to better reveal the movement law of overburden structures in the large-section withdrawal space under the conditions of whether the withdrawal space stops coal caving during the continuous advancement of the final mining face and better guides the field engineering practice, a physical similarity model is established to simulate the typical stopping coal caving operation. The geometric similarity ratio of the model is 100:1, the size of the support is 1.8 m × 0.2 m × 1.4 m, the thickness of the rock layer is 112.3 cm,

the thickness of the coal seam is 19.0 cm, the height of the hydraulic support is 3.5 cm, the bulk density similarity ratio is 1.6:1, and the time similarity ratio is 10:1. The migration of overlying rock structure under the typical stopping distance of coal caving is shown in Figure 13.

(1) In the early stage of the similar simulation experiment, the thickness of the normal mining coal seam before the excavation of the withdrawal channel is 19.0 cm, that is, the stopping caving distance is 0 m (Figure 13b). Due to not stopping coal caving, the direct roof caving and crushing expansion did not fully fill the goaf, C_1 could not fully contact the direct roof caving filling area, and C_1 continued to rotate and sink. At the same time, B breaks above the support area for the hydraulic support, and there is a large range of suspended roof area below B. The overlap width between B and the stopping coal pillar decreases, and the vertical drop between B and C_1 is large. A stable hinged structure cannot be maintained for a long time between A, B, and C_1. The rotation angle of B is large, and most of the sinking extrusion force acts on the top of the withdrawal space, and the hydraulic support is seriously deformed.

(2) The working face continues to advance but only 3.5 cm coal seam is mined. The designed span of non-top coal is 30 m, that is, the distance of stopping coal caving is 30 m (Figure 13c). C_2 and C_3 are in full contact with the direct roof caving filling area, and uncaving the top coal and direct roof caving fully fills the goaf; then, B and C_1 are in full contact with the coal and rock mass in the filling area, and the rotation angle of B and C_1 is small. At the same time, the fracture position of the main roof is located above the goaf. Most of the rotary extrusion pressure of B acts on the stopping coal caving filling area, and the withdrawal space is placed below the A region. At this time, the support control of the withdrawal space is not difficult, and the withdrawal space is slowly and stably deformed, which can ensure the safe and efficient withdrawal of the support.



(**a**)

Figure 13. *Cont.*

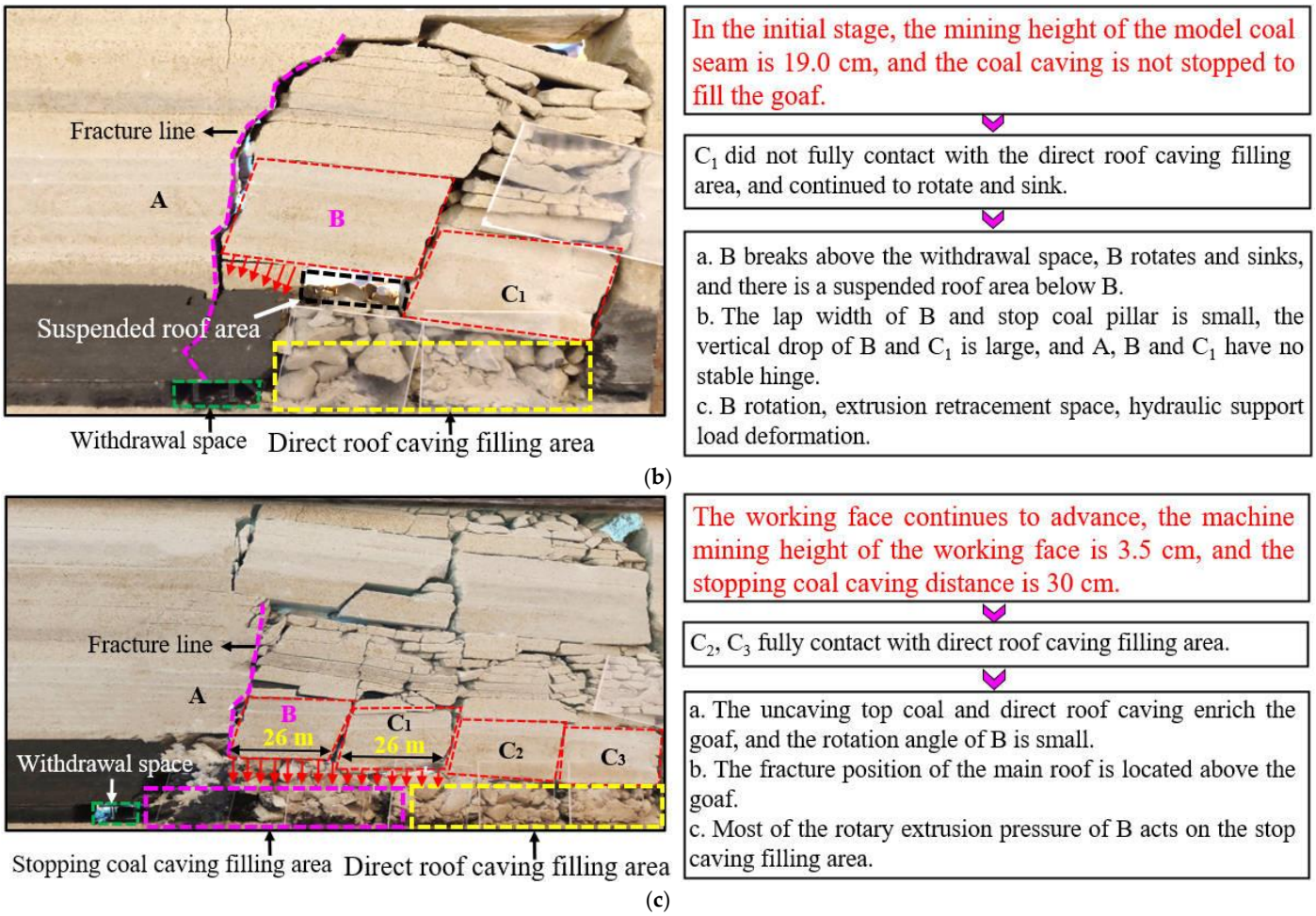


Figure 13. Migration characteristics of overburden structures in withdrawal space under typical stopping coal caving distance: (**a**) the whole picture of similar simulation model; (**b**) L_C = 0 m; (**c**) L_C = 30 m. The red font is to highlight the message that different pictures want to convey.

5. Asymmetric Partition Support Monitoring System for the Final Mining Withdrawal Space

5.1. Asymmetric Support Control Scheme of the Final Mining Withdrawal Space Partition

Due to the influence of many factors such as the geological structure and mining disturbance of the working face, the degree of plastic damage of the surrounding rock in front of and behind the final mining face is obviously different. The distribution of overburden rock and stress shows obvious zoning characteristics, that is, the stopping coal caving area, the support area of the hydraulic support, the withdrawal channel area, and the stopping coal pillar area.

(1) The reasonable space–time layout of the withdrawal space under the scientific stopping coal caving distance and the basic roof fracture position in the stopping coal pillar area ensures that most of the dynamic and static load stresses of the overlying strata act on the caving direct roof and the loose top coal to improve the stress environment of the withdrawal space overburden.

(2) The withdrawal space is divided into the support area of the hydraulic support and withdrawal channel area. It can be seen from the stress distribution cloud diagram that the vertical stress depressor area and the maximum shear stress low-value area of the surrounding rock in the support area of the hydraulic support are large but the roof of the area needs to have a certain bearing capacity to ensure that the top coal will not fall close to the support and the roof will not collapse with the withdrawal of the

support; therefore, the strength of the roof in the support area should not be too large. The withdrawal channel area is the key point of the whole withdrawal space support. Therefore, in the design scheme, the anchor cable must pass through the low-value area of the maximum shear stress combined with the bolt to tighten the plasticized coal body, and the anchor cable is anchored to the range of the maximum shear stress increase area. The anchor depth at the shoulder socket of the withdrawal channel also needs to reach the range of the maximum shear stress increase area. Therefore, the inclined anchor cable is used at the shoulder socket of the withdrawal channel area and a row of single hydraulic props are set up at 400 mm from the coal wall of the withdrawal channel to prevent the risk of end mining and roof cutting.

(3) The vertical stress depressor area and the maximum shear stress low-value zone of the stopping coal pillar area are small and the support requirements are not high as long as the coal wall does not occur in a large area.

Based on the typical zoning characteristics of the withdrawal space, an asymmetric zoning support control scheme for the final mining withdrawal space is proposed as shown in Figure 14.

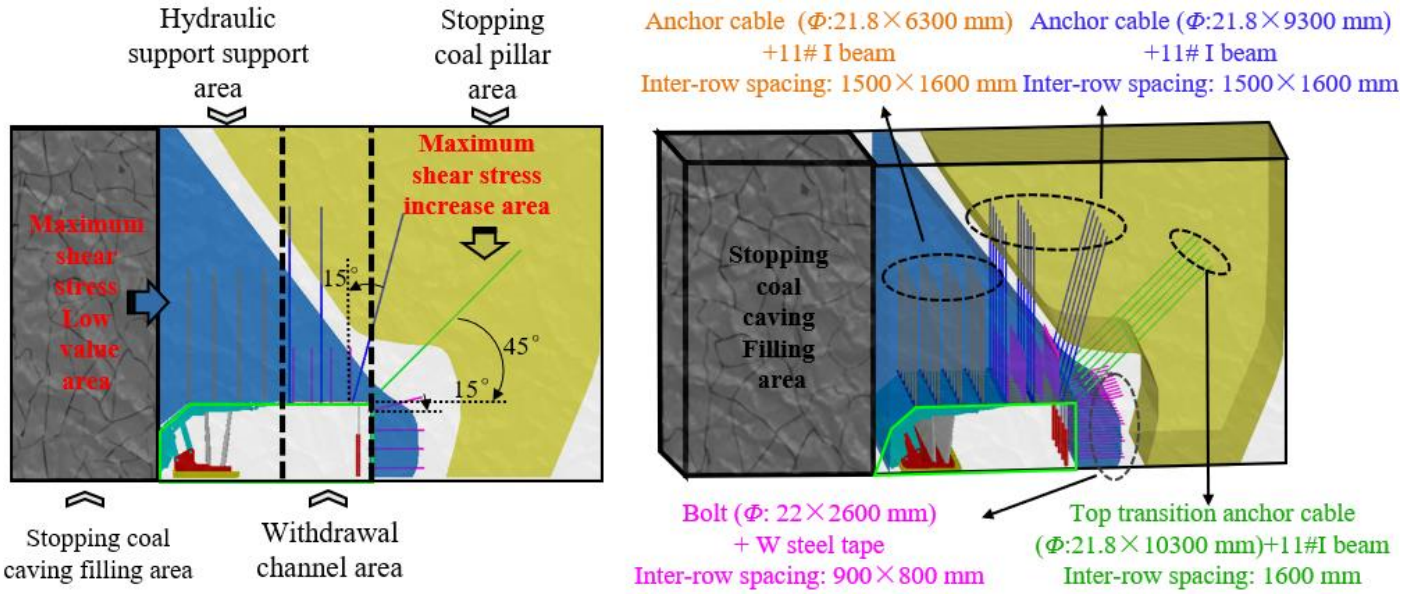


Figure 14. Asymmetric partition support control scheme for final mining withdrawal space. Different colors represent different support zones.

5.2. Simulation Analysis of the Pre-Stress Field of the Withdrawal Space Partition Support

In order to verify the scientificity of the partition support control in the withdrawal space and to check the support scheme reasonably, the pre-stress field model of the partition support is established as shown in Figure 15.

Through the analysis of pre-stressed simulation results, it can be seen that the set of partition support design schemes forms a 0.02 MPa continuous anchorage bearing arch structure in the deep anchorage zone of the top coal anchor cable, and the combined support of bolt and cable forms a high pre-stressed anchorage bearing arch with a boundary of 0.2 MPa in the shallow coal body of top coal. The roof bolt–cable synergistic anchoring range of the withdrawal channel area is large, the high pre-stressed area is connected, and the pre-tightening anchoring effect is better than the roof of the support area for the hydraulic support. From the perspective of the pre-stressed field in the large-section withdrawal space, the roof of the support area for the hydraulic support, the roof of the withdrawal channel area, and the top-to-side transition area form a large-scale high-pre-

stressed field penetration area, and the support strength meets the needs of the partition support control.

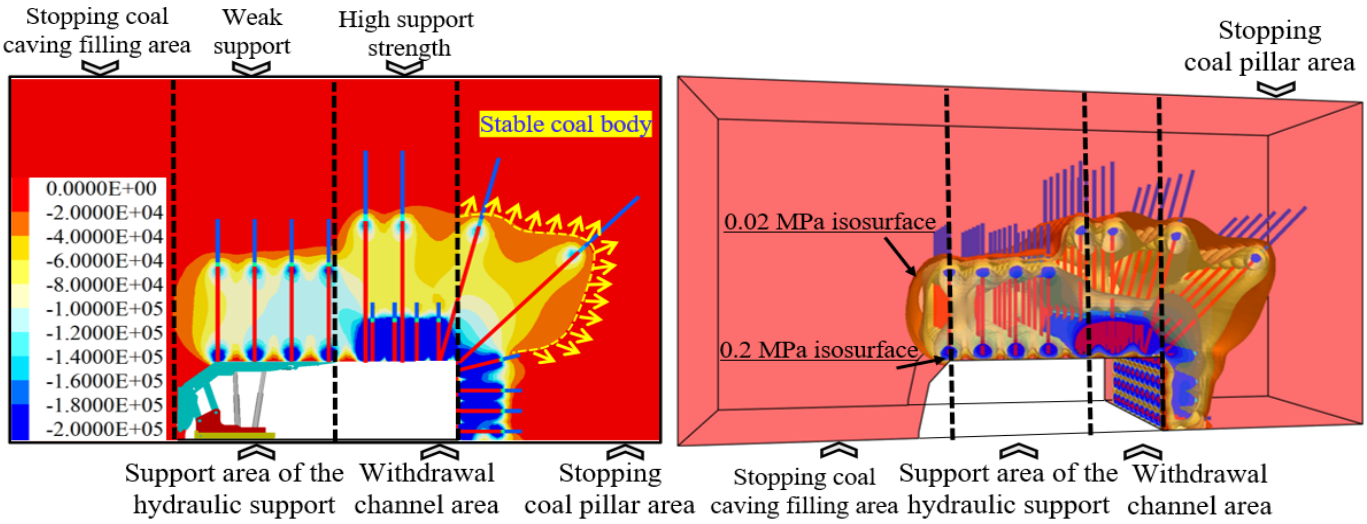
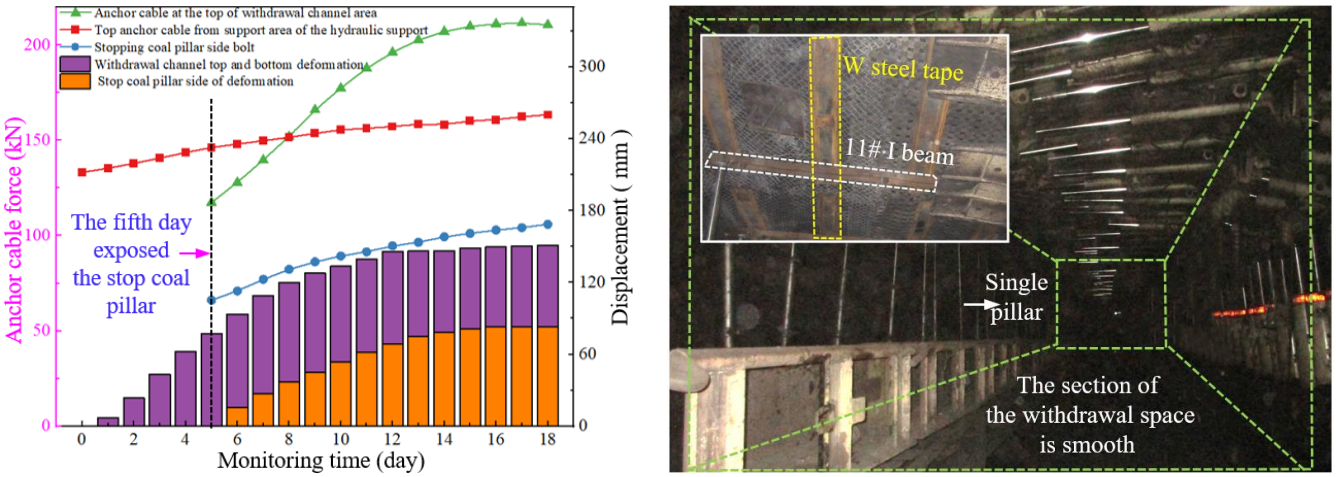


Figure 15. Pre-stressed field model of asymmetric partition support.

5.3. Rock Pressure Monitoring of the Large-Section Withdrawal Space in the Final Mining Stage

The deformation of surrounding rock and the stress of the anchor cable from the beginning of roadway excavation to the withdrawal of the working face are shown in Figure 16a. The maximum roof subsidence of the withdrawal space is 151 mm. The withdrawal space is completed on the fifth day and the stopping coal pillar is revealed. The maximum deformation of the stopping coal pillar is 82 mm before the withdrawal, and the deformation of the top wall meets the requirements of the safe and rapid withdrawal operation in the later period.



(**a**) (**b**)

Figure 16. Mine pressure monitoring in withdrawal space: (**a**) the deformation of surrounding rock and the stress of anchor cable; (**b**) on site support control effect.

The force of the top anchor cable in the withdrawal channel before the withdrawal of the support is 210 kN, the force of the top anchor cable in the support area of the hydraulic support is 163 kN, and the force of the anchor bolt in the stopping coal pillar is 106 kN. Obviously, the anchor cable shows a good anchoring effect but the change rate of anchorage

force of the anchor cable on the roof of withdrawal channel is fast, the strength of the top anchor cable in the withdrawal channel area is better than that of the top anchor cable in the support area of the hydraulic support, which is in line with the principle of asymmetric partition support control in the final mining withdrawal space.

The effect diagram of the on site support control is shown in Figure 16b. The section of the withdrawal space in the preparation and withdrawal sections of the working face remains flat, and there is no strong mine pressure phenomenon such as roof fall, rib spalling, support member failure, and support crushing in the roadway, which fully meets the needs of safe and efficient withdrawal in the later periods.

In conclusion, the monitoring and support control measures have proven to be effective in managing the deformation and stress levels in the withdrawal space. The data collected and the subsequent adjustments made to the support system have ensured that the mining operation can proceed safely and efficiently, with the structural integrity of the roadway being maintained throughout the withdrawal process. This success is a testament to the careful planning and execution of the support strategy, which has been designed to accommodate the unique challenges of the final mining withdrawal space.

6. Conclusions

(1) According to the migration characteristics of overlying strata in the withdrawal space under different stopping coal caving distances in the working face, different stopping coal caving distances are divided into four stopping coal caving spans. Utilizing the theoretical analysis method, we have ascertained that a suitable stopping coal caving span should be within the range of 1 to 2 times the cycle weighting interval, and the optimal stopping coal caving distance is 30 m. Moreover, the "S-R" stability theory, which pertains to the "masonry beam" structure, has been employed to illustrate that at a stopping coal caving distance of 30 m, the critical blocks of the main roof are stable, with neither rotational nor sliding instability occurring between them.

(2) Numerical simulation is used to analyze the migration of the overburden structure, vertical stress, and maximum shear stress evolution characteristics of the withdrawal space under different stopping caving distances and different fracture positions of the main roof. It is concluded that the overburden and stress distribution of the withdrawal space have obvious zoning characteristics, that is, the stopping coal caving filling area, the support area of the hydraulic support, the withdrawal channel area, and the stopping coal pillar area. When the distance of stopping coal caving is 30 m and the fracture position of the main roof is located above the goaf, the range of the stress reduction area of coal and rock mass on the side of the withdrawal space and stopping coal pillar is greatly reduced, and the coal and rock mass still has good bearing and shear resistance.

(3) The physical similarity model of the withdrawal space of the final mining under the typical stopping coal caving distance (0 m, 30 m) is constructed. The results show that the reasonable stopping coal caving can fully fill the goaf under B and part of C_1, slow down the rotation angle of B and C_1 and the difficulty of the withdrawal space support, and protect the safe and efficient withdrawal of the support.

(4) Based on the typical zoning characteristics of the withdrawal space overburden, an asymmetric zoning support control scheme for the withdrawal space is proposed. The real-time monitoring results of surrounding rock deformation show that the maximum roof subsidence in the withdrawal space is 151 mm and the maximum deformation of the stopping coal pillar is 82 mm. The anchoring strength of the anchor cable at the top of the withdrawal channel area > the anchoring strength of the anchor cable in the support area of the hydraulic support > the anchoring strength of the stopping coal pillar area. The deformation of the section of the withdrawal space meets the needs of safe and efficient withdrawal for the final mining stages.

Author Contributions: Writing—original draft preparation, D.C. and Z.W.; writing—review and editing, D.C., S.Y., S.X. and F.H.; supervision, C.T. and Z.J.; funding acquisition, S.Y., D.C., S.X., F.H. and Z.J.; data curation, Z.W., D.L. and B.Q. All authors have read and agreed to the published version of the manuscript.

Funding: This research was funded by the Natural Science Foundation of Henan Province (No. 222300420170), the National Natural Science Foundation of China (No. 52004286), the National Natural Science Foundation of China (No. 52374149), the National Natural Science Foundation of China (No. 52074296), and the Fundamental Research Funds for the Central Universities (Ph.D. Top Innovative Talents Fund of CUMTB) (No. BBJ2024007).

Data Availability Statement: The datasets generated or analyzed during the current study are available from the corresponding author upon reasonable request.

Acknowledgments: All the authors thank the above funds for their sponsorship support and thank the on-site technical personnel for their geological data sharing and test support.

Conflicts of Interest: The authors declare that they have no conflicts of interest.

References

1. Wu, Z.Y.; Sun, Q.; Wang, Y.B. Evolution laws of water-flowing fracture zone and mine pressure in mining shallow-buried, hard, and extra-thick coal seams. *Appl. Sci.* **2024**, *14*, 2915. [CrossRef]
2. Chen, D.D.; Zhu, J.K.; Ye, Q.C.; Ma, X.; Xie, S.R.; Guo, W.K.; Li, Z.J.; Wang, Z.Q.; Feng, S.H.; Yan, X.X. Application of gob-side entry driving in fully mechanized caving mining: A review of theory and technology. *Energies* **2023**, *16*, 2691. [CrossRef]
3. Pan, W.D.; Zhao, Z.N.; Li, X.Y.; Xu, Y.X.; Zhang, K.M. Top coal drawing law for an extra thick coal seam under the single round group drawing method. *Sci. Rep.* **2024**, *14*, 15293. [CrossRef]
4. Sun, X.M.; Zhao, W.C.; Wang, J.; Jiang, M.; Shen, F.X.; Zhang, Y.; Miao, C.Y. Research on failure mechanism and stability control technology of dynamic pressure roadway in ultra-thick coal seams under a high depth of cover. *Min. Metall. Explor.* **2023**, *40*, 1955–1972. [CrossRef]
5. Wang, Q.; Jiang, Z.H.; Jiang, B.; He, M.C.; Yang, J.; Xue, H.J. Ground control method of using roof cutting pressure release and energy-absorbing reinforcement for roadway with extra-thick hard roof. *Rock Mech. Rock Eng.* **2023**, *56*, 7197–7215. [CrossRef]
6. Yan, H.; Zhang, J.X.; Feng, R.M.; Wang, W.; Lan, Y.W.; Xu, Z.J. Surrounding rock failure analysis of retreating roadways and the control technique for extra-thick coal seams under fully-mechanized top caving and intensive mining conditions: A case study. *Tunn. Undergr. Space Technol.* **2020**, *97*, 103241. [CrossRef]
7. Biały, W.; Prostański, D.; Bołoz, Ł. Selection of longwall shearers based on the results of research on the mechanical properties of coal. *Sci. Rep.* **2024**, *14*, 18606. [CrossRef]
8. Yang, Y.; Qingliang, Z.; Qiang, Z. Analysis of coal gangue recognition capability based on vibration characteristics of the tail beam and experimental study on coal gangue recognition in fully mechanized top coal caving. *Int. J. Coal Prep. Util.* **2024**, *44*, 953–974. [CrossRef]
9. Shan, P.F.; Yang, T.; Wu, X.C.; Sun, H.Q. A research study of lightweight state perception algorithm based on improved yolov5s-tiny for fully mechanized top-coal caving mining. *Energy Sci. Eng.* **2024**, *12*, 2864–2878. [CrossRef]
10. Guan, Z.L.; Liu, W.L. Multi-frequency gpr data fusion through a joint sliding window and wavelet transform-weighting method for top-coal structure detection. *Appl. Sci.* **2024**, *14*, 2721. [CrossRef]
11. Zhu, Y.P.; Zeng, Q.H.; Wan, L.; Yang, Y.R.; Li, Z. Vibration response difference of caving mechanism under coal rock impact based on mechanical-hydraulic coupling. *Sci. Rep.* **2023**, *13*, 13794. [CrossRef] [PubMed]
12. Zhang, N.B.; Liu, C.Y.; Yang, P.J. Flow of top coal and roof rock and loss of top coal in fully mechanized top coal caving mining of extra thick coal seams. *Arab. J. Geosci.* **2016**, *9*, 465. [CrossRef]
13. Chen, D.D.; Jiang, Z.S.; Ma, X.; Xie, S.R.; Wang, E.; Li, H. Evolution law and engineering application on main stress difference for a novel stress relief technology in two ribs on deep coal roadway. *J.Cent. South Univ.* **2023**, *30*, 2266–2283. [CrossRef]
14. Hao, J.; Chen, A.F.; Li, X.L.; Bian, H.; Zhou, G.H.; Wu, Z.G.; Peng, L.J.; Tang, J.Q. Analysis of surrounding rock control technology and its application on a dynamic pressure roadway in a thick coal seam. *Energies* **2022**, *15*, 9040. [CrossRef]
15. Hu, S.X.; Ma, L.Q.; Guo, J.S.; Yang, P.J. Support-surrounding rock relationship and top-coal movement laws in large dip angle fully-mechanized caving face. *Int. J. Min. Sci. Technol.* **2018**, *28*, 533–539.
16. Xie, S.R.; Wu, Y.Y.; Chen, D.D.; Liu, R.P.; Ham, X.T.; Ye, Q.C. Failure analysis and control technology of intersections of large-scale variable cross-section roadways in deep soft rock. *Int. J. Coal Sci. Technol.* **2022**, *9*, 19. [CrossRef]
17. Zhou, Y.; Yu, X.Y. Study of the evolution of water-conducting fracture zones in overlying rock of a fully mechanized caving face in gently inclined extra-thick coal seams. *Appl. Sci.* **2022**, *12*, 9057. [CrossRef]
18. Vu, T.T. Solutions to prevent face spall and roof falling in fully mechanized longwall at underground mines, Vietnam. *Min. Miner. Depos.* **2022**, *16*, 127. [CrossRef]
19. Ma, X.; Chen, D.D.; Xie, S.R.; Zou, J.; Wu, H.D.; Sun, A.G.; Wang, Z.Q. Failure Mechanism of Severe Deformation in Gob-Side Entry Rib and Unloading-Supporting Coupling Control Technology. *Eng. Fail. Anal.* **2025**, *167*, 108973. [CrossRef]

20. Xie, G.X.; Chang, J.C.; Yang, K. Investigations into stress shell characteristics of surrounding rock in fully mechanized top-coal caving face. *Int. J. Rock Mech. Min.* **2009**, *46*, 172–181. [CrossRef]
21. Lv, H.Y.; Cheng, Z.B.; Liu, F. Study on the mechanism of a new fully mechanical mining method for extremely thick coal seam. *Int. J. Rock Mech. Min.* **2021**, *142*, 104788. [CrossRef]
22. Sakhno, I.; Sakhno, S. Numerical studies of floor heave mechanism and the effectiveness of grouting reinforcement of roadway in soft rock containing the mine water. *Int. J. Rock Mech. Min.* **2023**, *170*, 105484. [CrossRef]
23. Wang, H.W.; Wu, Y.P.; Jiao, J.Q.; Cao, P.P. Stability mechanism and control technology for fully mechanized caving mining of steeply inclined extra-thick seams with variable angles. *Min. Metall. Explor.* **2021**, *38*, 1047–1057.
24. Cui, F.; Lei, Z.Y.; Chen, J.Q.; Chang, B.; Yang, Y.B.; Li, C.L.; Jia, C. Research on reducing mining-induced disasters by filling in steeply inclined thick coal seams. *Sustainability* **2019**, *11*, 5802. [CrossRef]
25. Kong, D.Z.; Pu, S.J.; Cheng, Z.H.; Wu, G.Y.; Liu, Y. Coordinated deformation mechanism of the top coal and filling body of gob-side entry retaining in a fully mechanized caving face. *Int. J. Geomech.* **2021**, *21*, 04021030. [CrossRef]
26. Li, S.; Fan, C.J.; Luo, M.K.; Yang, Z.H.; Lan, T.W.; Zhang, H.F. Structure and deformation measurements of shallow overburden during top coal caving longwall mining. *Int. J. Min. Sci. Technol.* **2017**, *27*, 1081–1085. [CrossRef]
27. Tu, M.; Bu, Q.W.; Fu, B.J.; Wang, Y. Mechanical analysis of mining stress transfer on isolated island face in extra-thick fully mechanized top-coal caving mining. *Geofluids* **2020**, *2020*, 8834321. [CrossRef]
28. Zhao, Y.Q.; Yang, Y.M.; Li, X.B.; Wang, Z.Q. Overlying strata movement and abutment pressure evolution process of fully mechanized top coal caving mining in extra thick coal seam. *Geofluids* **2021**, *2021*, 7839888. [CrossRef]
29. Xu, X.H.; He, F.L.; Li, X.B.; He, W.R. Research on mechanism and control of asymmetric deformation of gob side coal roadway with fully mechanized caving mining. *Eng. Fail. Anal.* **2021**, *120*, 105097. [CrossRef]
30. Yan, S.H.; Shen, Y.P. Quantitative study on piled state of collapse top coal and drawing ratio in longwall with top coal caving. *J. Min. Saf. Eng.* **2023**, *40*, 656–667.
31. Qian, M.G.; Miao, X.X.; He, F.L. Analysis of key block in the structure of voussoir beam in longwall mining. *J. China Coal Soc.* **1994**, *19*, 557–563.

Disclaimer/Publisher's Note: The statements, opinions and data contained in all publications are solely those of the individual author(s) and contributor(s) and not of MDPI and/or the editor(s). MDPI and/or the editor(s) disclaim responsibility for any injury to people or property resulting from any ideas, methods, instructions or products referred to in the content.